

# Positivity violations in marginal structural survival models with time-dependent confounding: a simulation study on IPTW-estimator performance

Marta Spreafico

[m.spreafico@math.leidenuniv.nl](mailto:m.spreafico@math.leidenuniv.nl)

*Mathematical Institute, Leiden University, Leiden 2333 CC, The Netherlands*

*Department of Biomedical Data Sciences, Leiden University Medical Center, Leiden 2333 ZA, The Netherlands*

January 13, 2025

## Abstract

In longitudinal observational studies, marginal structural models (MSMs) are a class of causal models used to analyse the effect of an exposure on the (time-to-event) outcome of interest, while accounting for exposure-affected time-dependent confounding. In the applied literature, inverse probability of treatment weighting (IPTW) has been widely adopted to estimate MSMs. An essential assumption for IPTW-based MSMs is the positivity assumption, which ensures that, for any combination of measured confounders among individuals, there is a non-zero probability of receiving each possible treatment strategy. Positivity is crucial for valid causal inference through IPTW-based MSMs, but is often overlooked compared to confounding bias. Positivity violations may also arise due to randomness, in situations where the assignment to a specific treatment is theoretically possible but is either absent or rarely observed in the data, leading to near violations. These situations are common in practical applications, particularly when the sample size is small, and they pose significant challenges for causal inference. This study investigates the impact of near-positivity violations on estimates from IPTW-based MSMs in survival analysis. Two algorithms are proposed for simulating longitudinal data from hazard-MSMs, accommodating near-positivity violations, a time-varying binary exposure, and a time-to-event outcome. Cases of near-positivity violations, where remaining unexposed is rare within certain confounder levels, are analysed across various scenarios and weight truncation (WT) strategies. This work aims to serve as a critical warning against overlooking the positivity assumption or naively applying WT in causal studies using longitudinal observational data and IPTW.

**Keywords:** inverse probability of treatment weighting; marginal structural models; positivity assumption; survival outcome; simulation studies.

## 1 Introduction

In longitudinal observational studies, exposure-affected time-varying confounding represents a specific challenge for estimating the effect of a treatment on the (time-to-event) outcome of interest, as standard analyses fail to give consistent estimators (Daniel et al., 2013; Clare et al., 2019). In the past decades considerable progresses have been made in developing causal methods for analysing such complex longitudinal data. Marginal Structural Models (MSMs) were introduced as a powerful method for confounding control in longitudinal studies (Daniel et al., 2013; Robins et al., 2000; Hernán et al., 2000; Williamson and Ravani, 2017), alternatively to structural nested models (Robins et al., 1992). MSMs are models for the *potential* or *counterfactual* outcome that individuals would have experienced if they had received a particular treatment or exposure value. This study focuses on counterfactual time-to-event outcomes by considering marginal structural hazard models (hazard-MSM) or a discrete-time analogue. The parameters of a MSM can be consistently estimated through various methods, including Inverse Probability

of Treatment Weighting (IPTW) estimators, G-computation, or doubly robust methods (Daniel et al., 2013; Clare et al., 2019; Robins et al., 2000; van der Laan and Gruber, 2016; Hernán and Robins, 2020; Gabriel et al., 2024). Despite less robust, IPTW-based MSMs have largely been adopted in the applied literature, especially in epidemiology and medicine, due to its simplicity in both implementation and interpretation (Clare et al., 2019). IPTW-based MSMs require the correct specification of the exposure model conditional on confounders (i.e., the *weighting model*) and special attention to the identifiability assumptions of consistency, no unmeasured confounding, and positivity (Hernán and Robins, 2020; Cole and Hernán, 2008; Cole and Frangakis, 2009; Williamson and Ravani, 2017). This work focuses on the latter, which is often overlooked compared to confounding bias.

Positivity holds if, for any combination of the measured confounders occurring among individuals in the population, there is a non-zero (i.e., positive) probability of receiving every level of the exposure possible under the target treatment strategies to be compared (Cole and Hernán, 2008; Hernán and Robins, 2020). While less well-recognized than bias due to incomplete control of confounding, violations of the positivity assumption can increase both the variance and bias of causal effect estimates (Petersen et al., 2012; Léger et al., 2022). Positivity violations can occur in two situations (Zhu et al., 2021). *Strict* (or *theoretical*) violations occur when certain treatment levels are impossible for specific subgroups of subjects. For example, if a certain treatment  $a$  is never given to individuals with severe comorbidities, then the causal effect of  $a$  cannot be estimated for that subgroup; the analysis should therefore focus only on individuals without severe comorbidities. Even in the absence of structural zeros, *random* zeros may occur by chance due to small sample sizes or highly stratified data by numerous confounders. *Near* (or *practical*) violations refer to situations where the assignment to a specific treatment is always theoretically possible but is not (or rarely) observed in the data due to randomness. Sampling variability may indeed result in subjects having a near-zero probability of being exposed (or unexposed) for certain combinations of covariate values. These situations are common in practical applications, particularly when the sample size is small, and they pose significant challenges for causal inference. While treatment remains technically possible within a subgroup, its rarity makes reliable estimation difficult, particularly when using IPTW. Extremely small probabilities lead to extreme weights, which can destabilize the analysis and inflate variance. To address these challenges and stabilize the variance of estimates, Weight Truncation (WT) is often applied in IPTW to down-weight observations in regions where near-violations occur (Cole and Hernán, 2008; Xiao et al., 2013; Zhu et al., 2021). However, if applied inappropriately, this technique could result in excessive truncation, which may introduce bias into the estimates.

In the literature, research studies on positivity violations have been previously carried out in a pedagogical manner by using real data to illustrate how incorrect inference occurs in estimating MSMs when positivity is violated (Mortimer et al., 2005; Bembom and van der Laan, 2007; Cole and Hernán, 2008; Zhu et al., 2021; Rudolph et al., 2022; Zhu et al., 2023). Findings from different studies agreed that positivity violations have a more severe impact for the IPTW-estimator than other causal estimators. However, when using real data, disentangling the effect of positivity violations from other sources of bias is typically not possible: important confounders may be undetected or unmeasured and the fulfilment of the remaining assumptions underlying the IPTW-estimator is generally difficult to ascertain. Moreover, real data do not allow us to design scenarios that could be of interest, such as studying performance under different sample sizes. To overcome these limitations, other investigations were conducted more systematically by setting up simulation studies (Neugebauer and van der Laan, 2005; Wang et al., 2006; Naimi et al., 2011; Petersen et al., 2012; Léger et al., 2022). Results confirmed that under positivity violations IPTW-estimator performs worse than other methods, becoming very unstable and exhibiting high variability. However, these studies were limited to assessing the causal effect of a treatment assigned either at a single time point or twice.

This study investigates the impact of near-positivity violations on the performance of IPTW-estimated MSMs in longitudinal survival contexts with time-varying confounding using a simulation-based approach. No systematic simulation studies currently exist in this framework, largely due to the challenges of simulating longitudinal survival data under conditions of both exposure-affected time-varying confounding and near-positivity violations. To address this gap, two algorithms are proposed for simulating longitudinal data from hazard-MSMs, accommodating near-positivity violations, a time-varying binary exposure, and a survival outcome. These methods build on the works of Havercroft and Didelez (2012) and Keogh et al. (2021). Two simulation studies analysing cases of near-positivity violations, where remaining unexposed is rare within certain levels of confounders, through various scenarios and WT strategies are performed.

This study aims to highlight the critical importance of carefully considering the positivity assumption

in causal studies that utilize longitudinal observational data and IPTW. The final purpose is to warn against the risks of underestimating the assumption’s significance or uncritically applying WT methods. This is fundamental given that the past several decades have seen an exponential growth in causal inference approaches and their applications to observational data (Hammerton and Munafò, 2021; Mitra et al., 2022; Olier et al., 2023), including emerging areas such as target trial emulations (Hernán and Robins, 2016; Hernán, 2021), prediction modelling under hypothetical interventions (van Geloven et al., 2020; Lin et al., 2021; Keogh and van Geloven, 2024), or causal machine learning (Feuerriegel et al., 2024; Moccia et al., 2024).

This study is organized as follow. Section 2 briefly recalls the notation, MSMs for survival outcomes, and IPTW. Section 3 explains the proposed mechanism to enforce positivity violations in algorithms to simulate longitudinal data from MSMs. Sections 4 and 5 present the two simulation studies. Section 6 finally discusses the findings and provide recommendations. Statistical analyses were performed in the R software environment (R Core Team, 2023). Source code is available at <https://github.com/mspreafico/PosViolMSM>.

## 2 Marginal structural models for potential survival outcomes

### 2.1 Notation

Let us consider a set of  $i = 1, \dots, n$  subjects and a set of regular visits  $k = 0, 1, \dots, K$  performed at times  $q_0 < q_1 < \dots < q_K$  (assumed to be the same for everybody). Each subject undergoes each visit up until event time  $T_i^* = \min(C_i, T_i)$ , i.e., the earlier of the time of the actual event of interest  $T_i$  and the administrative censoring time  $C_i$ . At each visit  $k$ , a binary treatment status  $A_{i,k} \in \{0, 1\}$  (unexposed vs exposed; control vs treatment) and a set of time-dependent covariates  $L_{i,k}$  are observed. A bar over a time-dependent variable indicates the history, that is  $\bar{A}_{i,k} = (A_{i,0}, \dots, A_{i,k})$  and  $\bar{L}_{i,k} = (L_{i,0}, \dots, L_{i,k})$ . Finally, the binary failure indicator process is denoted by  $Y_{i,k+1}$ , where  $Y_{i,k+1} = 1$  if subject  $i$  has failed (e.g., died) in period  $(q_k; q_{k+1}]$ , i.e.,  $q_k < T_i \leq q_{k+1}$ , or  $Y_{i,k+1} = 0$  otherwise.

### 2.2 Marginal structural models for counterfactual hazard rates

Marginal structural hazards models (hazard-MSMs) are a class of causal models that focus on *counterfactual* time-to-event variables (Hernán et al., 2000; Robins et al., 2000; Hernán and Robins, 2020). These variables represent the time at which an event would have been observed had a patient been administered a specific exposure strategy  $\bar{a} = (a_0, a_1, \dots, a_K)$  with  $a_k \in \{0, 1\}$  for all  $k$ . Vector  $\bar{a}$  might differ from the actual treatment received  $\bar{A}_i = \bar{A}_{i,K} = (A_{i,0}, \dots, A_{i,K})$ . The *counterfactual event time* that would be observed in a subject under complete exposure history  $\bar{a}$  is denoted by  $T^{\bar{a}}$ . Hazard-MSMs hence model the counterfactual hazard rate:

$$\lambda^{\bar{a}}(t) = \lim_{\Delta t \rightarrow 0} \frac{P(t \leq T^{\bar{a}} < t + \Delta \mid T^{\bar{a}} \geq t)}{\Delta t}.$$

In case of discrete-time hazard of failure, a *marginal structural logistic regression model (logit-MSM)* can be assumed to model the counterfactual probability of failure in a single interval  $(q_k, q_{k+1}]$ , given survival up to  $q_k$ . The *logit-MSM* for the counterfactual hazard at visit  $k$  is defined as follows:

$$\lambda_k^{\bar{a}} = \Pr(Y_{k+1}^{\bar{a}} = 1 \mid Y_k^{\bar{a}} = 0) = \text{logit}^{-1}[\tilde{\gamma}_0 + g(\tilde{\gamma}_A; \bar{a}_k)], \quad (1)$$

where  $\bar{a}$  is the the complete treatment strategy,  $Y_k^{\bar{a}}$  is the counterfactual event indicator at visit  $k$ ,  $g(\cdot)$  is a function (to be specified) of the treatment strategy history up to visit  $k$  (denoted by  $\bar{a}_k$ ), and  $(\tilde{\gamma}_0, \tilde{\gamma}_A)$  is the vector of log odd ratios, with  $\tilde{\gamma}_0$  as the intercept.

In the context of continuous-time hazard, the *marginal structural Cox proportional hazard model (Cox-MSM)* form is often assumed to model the counterfactual hazard at time  $t$  given treatment history  $\bar{a}$ :

$$\lambda^{\bar{a}}(t) = \lambda_0(t) \exp \left\{ g \left( \tilde{\beta}_A; \bar{a}_{[t]} \right) \right\}, \quad (2)$$

where  $\lambda_0(t)$  is the baseline hazard function,  $\bar{a}_{[t]}$  denotes treatment pattern up to the most recent visit prior to time  $t$  (i.e.,  $[t] = \max_{k \leq t} k$ ),  $g(\cdot)$  is a function (to be specified) of treatment pattern  $\bar{a}_{[t]}$ , and

$\tilde{\beta}_A$  is a vector of log hazard ratios. An alternative often used is the *marginal structural Aalen's additive hazard model* (Aalen-MSM), defined as

$$\lambda^{\bar{\mathbf{a}}}(t) = \tilde{\alpha}_0(t) + g(\tilde{\alpha}_A(t); \bar{\mathbf{a}}_{[t]}) \quad (3)$$

where  $\tilde{\alpha}_0(t)$  is the baseline hazard at time  $t$ ,  $\bar{\mathbf{a}}_{[t]}$  denotes treatment pattern up to the most recent visit prior to time  $t$ ,  $g(\cdot)$  is a function (to be specified) of treatment pattern  $\bar{\mathbf{a}}_{[t]}$ , and  $\tilde{\alpha}_A(t)$  is the vector of coefficients at time  $t$ .

In the hazard-MSMs (1)-(3), the function  $g(\cdot)$  combines information from the treatment pattern up to the most recent visit  $k$  prior to time  $t$ . Depending on the desired information provided in  $g(\cdot)$ , the hazard at time  $t$  (or visit  $k$ ) can thus assume different forms. Table 1 shows examples of three forms of the treatment pattern function  $g(\cdot)$ , specifically: (i) the current level of treatment, (ii) the duration of treatment, or (iii) the history of treatment up to time  $t$  through the main effect terms for treatment at each visit. Any other desired form can be alternatively specified.

**Table 1:** Examples of treatment-pattern forms for function  $g(\cdot)$  in Equations (1) to (3).

Form of treatment pattern	Logit-MSM	Cox-MSM	Aalen-MSM
Function $g(\cdot)$	$g(\tilde{\gamma}_A; \bar{\mathbf{a}}_k)$ in (1)	$g(\tilde{\beta}_A; \bar{\mathbf{a}}_{[t]})$ in (2)	$g(\tilde{\alpha}_A(t); \bar{\mathbf{a}}_{[t]})$ in (3)
Current level of treatment	$\tilde{\gamma}_A \cdot a_k$	$\tilde{\beta}_A \cdot a_{[t]}$	$\tilde{\alpha}_A(t) \cdot a_{[t]}$
Duration of treatment	$\tilde{\gamma}_A \cdot \sum_{j=0}^k a_{k-j}$	$\tilde{\beta}_A \cdot \sum_{j=0}^{[t]} a_{[t]-j}$	$\tilde{\alpha}_A(t) \cdot \sum_{j=0}^{[t]} a_{[t]-j}$
Main effect terms at each visit	$\sum_{j=0}^k \tilde{\gamma}_{Aj} \cdot a_{k-j}$	$\sum_{j=0}^{[t]} \tilde{\beta}_{Aj} \cdot a_{[t]-j}$	$\sum_{j=0}^{[t]} \tilde{\alpha}_{Aj}(t) \cdot a_{[t]-j}$

### 2.2.1 Hazard-based estimands and marginal survival probabilities

The logit-MSM estimates log odd ratios  $\tilde{\gamma}_A$ , the Cox-MSM the log hazard ratios  $\tilde{\beta}_A$ , and the Aalen-MSM the cumulative regression coefficients  $\int_0^t \tilde{\alpha}_A(s) ds$ . Since hazard-based estimands may not have a straightforward interpretation, estimates from the MSMs are typically transformed into estimates for an interpretable causal estimand (Hernán, 2010; Martinussen et al., 2020; Keogh et al., 2021; Didelez and Stensrud, 2022). One example is comparing the marginal survival probabilities at time  $t$ , i.e.,  $S^{\bar{\mathbf{a}}}(t) = \Pr(T^{\bar{\mathbf{a}}} > t)$ , for *always treated*  $\bar{\mathbf{a}} = \mathbf{1} = (1, \dots, 1)$  (i.e., sustained use of the treatment) versus *never treated*  $\bar{\mathbf{a}} = \mathbf{0} = (0, \dots, 0)$  (i.e., sustained non-use of the treatment), or evaluating the marginal risk difference between them. The marginal survival probability at time  $t$  under treatment history  $\bar{\mathbf{a}}$  can be computed based on the different hazard forms:

(i) for the logit-MSMs in (1) is given by

$$S^{\bar{\mathbf{a}}}(t) = \prod_{k \leq t} (1 - \lambda_k^{\bar{\mathbf{a}}}) = \prod_{k \leq t} (1 - \text{logit}^{-1}[\tilde{\gamma}_0 + g(\tilde{\gamma}_A; \bar{\mathbf{a}}_k)]); \quad (4)$$

(i) for the Cox-MSM in (2) is given by

$$S^{\bar{\mathbf{a}}}(t) = \exp \left( -e^{g(\tilde{\beta}_A; \bar{\mathbf{a}}_0)} \int_0^1 \lambda_0(s) ds - e^{g(\tilde{\beta}_A; \bar{\mathbf{a}}_1)} \int_1^2 \lambda_0(s) ds - \dots - e^{g(\tilde{\beta}_A; \bar{\mathbf{a}}_{[t]})} \int_{[t]}^t \lambda_0(s) ds \right); \quad (5)$$

(iii) for the Aalen-MSM in (3) is given by

$$S^{\bar{\mathbf{a}}}(t) = \exp \left( -\int_0^t \tilde{\alpha}_0(s) ds - \int_0^1 g(\tilde{\alpha}_A(s); \bar{\mathbf{a}}_0) ds - \int_1^2 g(\tilde{\alpha}_A(s); \bar{\mathbf{a}}_1) ds - \dots - \int_{[t]}^t g(\tilde{\alpha}_A(s); \bar{\mathbf{a}}_{[t]}) ds \right). \quad (6)$$



### 2.3 Inverse Probability of Treatment Weighting (IPTW)

In the presence of confounders, MSMs can be estimated from the observed data by applying a technique called inverse probability of treatment weighting (IPTW) (Hernán and Robins, 2020). IPTW involves weighting the contribution of each subject  $i$  by the inverse of the probability of receiving their actual exposure level given their confounding covariates. This process creates a pseudo-population where confounding is no longer present. To optimize the variance estimation, stabilized (or standardized) weights are usually preferred (Robins et al., 2000; Hernán et al., 2000; Hernán and Robins, 2020; Léger et al., 2022). The stabilized weight for subject  $i$  at time  $t$  is defined as

$$sw_i(t) = \prod_{k=0}^{\lfloor t \rfloor} \frac{\Pr(A_{i,k} \mid \bar{A}_{i,k-1})}{\Pr(A_{i,k} \mid \bar{A}_{i,k-1}, \bar{L}_{i,k})}, \quad (7)$$

where  $\lfloor t \rfloor = \max_{k \leq t} k$  is the largest visit-time prior to  $t$ , and  $A_{-1}$  is defined to be 0. In the pseudo-population thus created, the effects of time-dependent confounding are balanced, so association in hazard regression models is causation (Hernán and Robins, 2020).

Even when standardized, weights  $sw_i(t)$  can largely inflate for a subject  $i$  concerned by near-positivity violation: when the denominator probabilities are very close to zero, weights become extremely large. In such cases, the common approach is to consider truncated stabilized weights  $\tilde{sw}_i(t)$  obtained by truncating the lowest and the highest estimations by the 1st and 99th (1-99) percentiles, or alternatively by narrower truncations, such as the 2.5-97.5, 5-95, or 10-90 percentiles (Cole and Hernán, 2008; Xiao et al., 2013; Zhu et al., 2021).

### 2.4 Simulating longitudinal survival data from marginal structural hazard models

Even when positivity holds, simulating longitudinal data when the model of interest is a model for potential outcomes, as for MSMs, is generally not straightforward (Evans and Didelez, 2023). The main challenges consist in: (i) replicating the complex dynamics of time-varying confounding; (ii) generating data in such a way that the model of interest is correctly specified; and (iii) in case of survival or other non-collapsible models (Robinson and Jewell, 1991; Didelez and Stensrud, 2022), reconciling the MSM with the conditional model used in Monte Carlo studies to generate the data. For these reasons, only a few methods for simulating data from hazard-MSMs have been published in the literature. These methods impose restrictions on the data-generating mechanisms to address the issues mentioned, allowing for accurate simulation of longitudinal data from pre-specified hazard-MSMs.

Xiao et al. (2010) and Young et al. (2010) first introduced two approaches for simulating from Cox-MSMs. Havercroft and Didelez (2012) and Young and Tchetgen Tchetgen (2014) outlined how to simulate in a discrete-time setting, from marginal structural logistic regression models and discrete-time Cox-MSMs, respectively. By finely discretizing time, these algorithms can be adapted to simulate from a continuous-time Cox-MSM. Keogh et al. (2021) introduced a method to simulate from a marginal structural Aalen’s additive hazard model that resulted in a less-restrictive generating mechanism. Recently, Seaman and Keogh (2024) outlined how to simulate from various hazard-MSMs that condition the hazard on baseline covariates.

Among these, the approaches by Havercroft and Didelez (2012) and Keogh et al. (2021) present similar structures of the temporal causal relationships between variables. The directed acyclic graphs (DAGs) in top panels of Figure 1 display for both cases the assumed data structure and inform which variables, measured at which time points, are confounders of the association between treatment at a given time point and the outcome. Both DAGs are illustrated in discrete-time for a follow-up with  $k = 0, \dots, K$  visits. Variables are assumed to be constant between visits. By imagining splitting the time intervals between successive visits into smaller and smaller intervals, both structures approach the continuous-time setting. For the current study, these two approaches are used as “truth” benchmarks for cases where longitudinal data generation from the desired hazard-MSM has already been demonstrated and positivity assumption is valid.

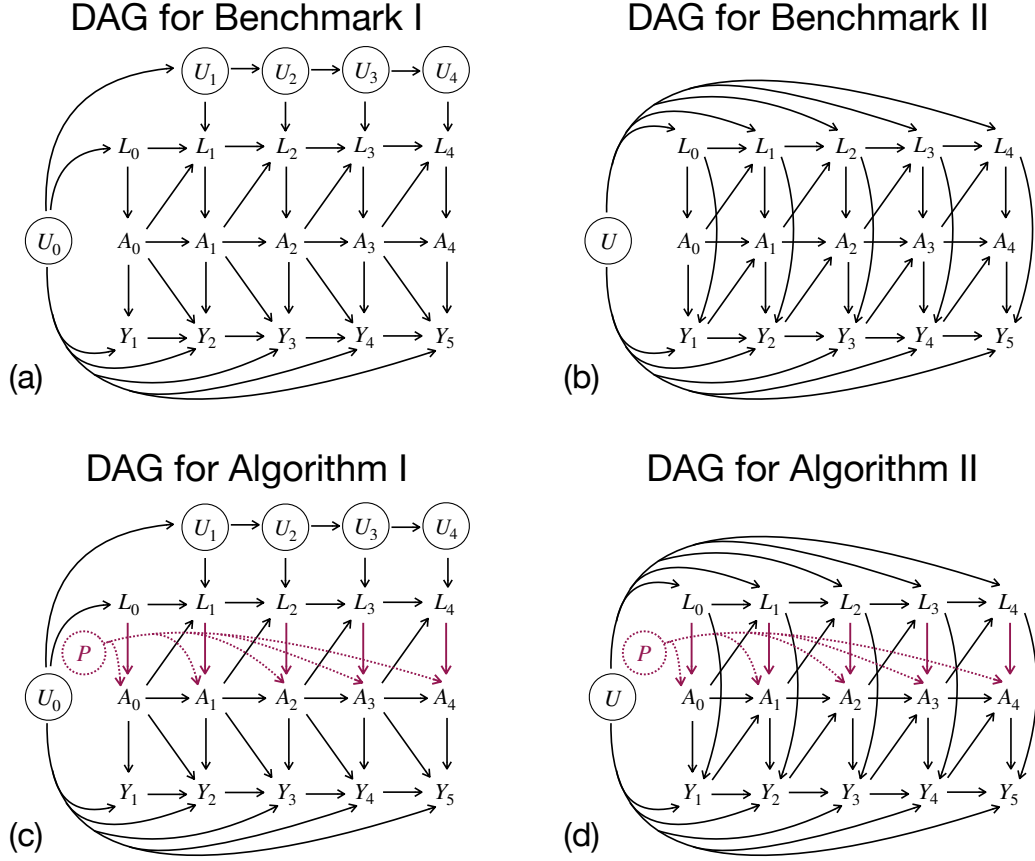


**Figure 1:** Top: Directed acyclic graphs (DAGs) illustrating the temporal causal relationships between variables in the data-generating mechanisms proposed by (a) [Havercroft and Didelez \(2012\)](#) and (b) [Keogh et al. \(2021\)](#), i.e., Benchmarks I and II. Bottom: DAGs illustrating the temporal causal relationships between variables in the proposed data-generating mechanisms, i.e., (c) Algorithm I and (d) Algorithm II.

### 3 Simulating longitudinal survival data with random positivity violations

To impose near-positivity violations within a data-generating mechanism, certain treatment levels (e.g., exposure or non-exposure in binary treatments) may become unobservable (though theoretically possible) for specific subgroups defined by confounders, due to randomness. Suppose the interest is on the subgroup of subjects presenting a poor health condition. Let us assume that the subgroup of subjects presenting a poor health condition at visit  $k$  is determined by a range of values  $\mathcal{I}_\tau$  of the confounder  $L_{i,k}$ . Near-positivity violations occur when the probability of remaining unexposed (or being exposed), given a poor health condition, is very close to zero (or approaches one):

$$\begin{aligned} \Pr(A_{i,k} = 0 \mid L_{i,k} = l_{i,k} \in \mathcal{I}_\tau, \bar{L}_{i,k-1} = \bar{l}_{k-1}, \bar{A}_{i,k-1} = \bar{a}_{k-1}) &\rightarrow 0, \\ \Pr(A_{i,k} = 1 \mid L_{i,k} = l_{i,k} \in \mathcal{I}_\tau, \bar{L}_{i,k-1} = \bar{l}_{k-1}, \bar{A}_{i,k-1} = \bar{a}_{k-1}) &\rightarrow 1, \end{aligned} \quad (8)$$

for all  $\bar{a}_{k-1}, \bar{l}_{k-1}$  when  $\Pr(\bar{A}_{i,k-1} = \bar{a}_{k-1}, \bar{L}_{i,k} = \bar{l}_k) \neq 0$ . This happens when remaining unexposed to treatment at visit  $k$  is rarely observable for subjects in the poor health subgroup.

Once defined the poor health subgroup of interest  $\mathcal{I}_\tau$ , violations occurring by chance can be introduced in a data generating mechanism by considering (i) a latent individual propensity  $P_i$  to exposure given a poor health condition, and (iii) an exposure cut-off  $\pi \in [0, 1]$ . For each subject  $i$ , a random uniform variable  $P_i$  is generated on the interval  $[0, 1]$  and treatment assignment is established by the exposure cut-off  $\pi$ . At each visit  $k$ , subjects in poor health with  $P_i \geq \pi$  are deterministically assigned to exposure and are considered positivity non-compliant. In contrast, subjects in poor health with  $P_i < \pi$  have a positive

probability of either receiving exposure or remaining unexposed and are considered positivity compliant. This leads to near-violations of the positivity assumption because, within the poor health subgroup defined by individuals  $i$  with  $L_{i,k} \in \mathcal{I}_\tau$ , both exposure and unexposure are theoretically possible. However, non-exposure may be rarely observed due to the randomness in drawing the individual propensities for exposure, creating situations where non-compliance with positivity occurs more frequently than expected, especially for low values of  $\pi$ .

The value  $\pi$  indeed represents the expected proportion of subjects for whom both exposure and non-exposure are observable in all subgroups defined by the measured confounder. In other words, it can be interpreted as the expected proportion of subjects compliant with positivity, and therefore:

- $\pi = 1$  means that all subjects are compliant with positivity, representing no positivity violations;
- $0 < \pi < 1$  means that  $\pi \times 100\%$  subjects are expected to be compliant with positivity, representing near-positivity violations;
- $\pi = 0$  means that all subjects are non-compliant with positivity, representing strict-positivity violations.

Therefore, for  $\mathcal{I}_\tau$  fixed, the higher the cut-off  $\pi$ , the less severe the violation.

Given an algorithm to simulate longitudinal survival data from MSMs in presence of time-varying confounding, near-positivity violations can be incorporated by using the pseudocode structure in panel Algorithm 1. The main advantage of imposing near-positivity violations in an existing approach, where longitudinal data generation from the desired hazard-MSM has already been confirmed, is the ability to directly examine the impact on IPTW estimators solely attributable to positivity violations, rather than other sources of bias. In this way, the original data-generating mechanism can be considered as the “truth” or benchmark case where the positivity assumption holds.

---

**Algorithm 1** General pseudocode for positivity violation.

---

```

Initialize parameters:  $(\mathcal{I}_\tau, \pi, \dots)$ 
for  $i = 1, \dots, n$  do
  ...
   $P_i \sim \mathcal{U}(0, 1)$  ▷ Draw the individual propensity
  for  $k = 0, \dots, K$  do
     $L_{i,k}$  is assigned based on the generating algorithm
    if  $P_i \geq \pi$  and  $L_{i,k} \in \mathcal{I}_\tau$  then
      exposure is assigned deterministically:  $A_{i,k} = 1$ 
    else
      exposure  $A_{i,k}$  is assigned stochastically based on the generating algorithm
    end if
  ...
end for
end for

```

---

## 4 Simulation study I

### 4.1 Data generation

The first algorithm proposed in this work is based on the data-generating mechanism introduced by [Havercroft and Didelez \(2012\)](#) to simulate from a discrete-time logit-MSM. This mechanism is now briefly introduced and then extended by imposing positivity violations.

#### 4.1.1 Benchmark I in a nutshell

Building upon the DAG in Figure 1a, [Havercroft and Didelez \(2012\)](#) proposed an algorithm to emulate longitudinal data from the Swiss HIV Cohort Study ([Sterne et al., 2005](#)). The authors considered a discrete-time setting where visit times correspond to visit numbers, i.e.,  $q_k = k$  for all  $k = 0, \dots, K$ .

The time-dependent binary treatment process  $A_{i,k}$  represents exposure to the highly active antiretroviral therapy (HAART) versus no treatment (unexposure). Once HAART has started for a subject  $i$ , it continues until failure or end of the follow-up period. The only measured time-dependent confounder  $L_{i,k}$  is the non-negative CD4 cell count, measured in *cells*/ $\mu L$ . Variable  $U_{i,k}$  represents the individual general latent health process, indicating a poor individual health status at visit  $k$  for values close to 0, or good health conditions for values close to 1. The latent process  $U_{i,k}$  and the survival process  $Y_{i,k+1} \in \{0, 1\}$  are updated at each time point  $k$ , whereas CD4 cell count  $L_{i,k} \geq 0$  and HAART exposure  $A_{i,k} \in \{0, 1\}$  are updated every  $\kappa$ -th time points, for a chosen  $\kappa$ , named check-up visits.

Despite there being no direct arrow from  $L_{i,k}$  to  $Y_{i,k+1}$ , the DAG (Figure 1a) exhibits time-dependent confounding due to  $U_{i,0}$  being a common ancestor of  $\bar{A}_i$  via  $\bar{L}_i$  and  $\bar{Y}_i$ . Moreover,  $A_{i,k}$  is independent from  $\bar{U}_{i,k}$  given  $(\bar{L}_{i,k}, \bar{A}_{i,k-1})$  and the vector  $\bar{L}_i$  is sufficient to adjust for confounding. Based on this mechanism, the authors proposed an algorithm to correctly simulate data from the following discrete-time logit-MSM:

$$\begin{aligned}\lambda_k^{\bar{a}} &= \text{logit}^{-1} [\tilde{\gamma}_0 + \tilde{\gamma}_{A1} \cdot \{(1 - a_k)k + a_k k^*\} + \tilde{\gamma}_{A2} \cdot a_k + \tilde{\gamma}_{A3} \cdot a_k(k - k^*)] \\ &= \text{logit}^{-1} [\tilde{\gamma}_0 + \tilde{\gamma}_{A1} \cdot d_{1k} + \tilde{\gamma}_{A2} \cdot a_k + \tilde{\gamma}_{A3} \cdot d_{3k}],\end{aligned}\quad (9)$$

where  $a_k$  is the binary treatment strategy at time  $k$ ,  $k^*$  is the treatment initiation time,  $d_{1k} = \min\{k, k^*\}$  and  $d_{3k} = \max\{k - k^*, 0\}$  represent the time elapsed before and after treatment initiation, respectively. Note that  $g(\tilde{\gamma}_A; \bar{a}_k) = \tilde{\gamma}_{A1} \cdot d_{1k} + \tilde{\gamma}_{A2} \cdot a_k + \tilde{\gamma}_{A3} \cdot d_{3k}$  in (9), reflecting that the hazard-MSM depends on a summary of the treatment history rather than only on the current treatment. In particular, Havercroft and Didelez proved that the parameters  $(\tilde{\gamma}_0, \tilde{\gamma}_{A1}, \tilde{\gamma}_{A2}, \tilde{\gamma}_{A3})$  in the desired logit-MSM (9) are collapsible with the conditional distribution parameters  $(\gamma_0, \gamma_{A1}, \gamma_{A2}, \gamma_{A3})$  in the following conditional logit model:

$$\lambda_{i,k} = \text{logit}^{-1} [\gamma_0 + \gamma_{A1} \cdot \{(1 - A_{i,k})k + A_{i,k} K_i^*\} + \gamma_{A2} \cdot A_{i,k} + \gamma_{A3} \cdot A_{i,k}(k - K_i^*)], \quad (10)$$

where  $K_i^*$  is the individual treatment initiation time, and  $\lambda_{i,k}$  represents the individual probability of failure in the interval  $k < t \leq k + 1$  conditional on survival up to visit  $k$ .

#### 4.1.2 Algorithm I: imposing random positivity violations in Benchmark I

As illustrated in the DAG in Figure 1c, the first proposed algorithm to account for potential near-positivity violations builds upon Benchmark I (Figure 1a) by incorporating two additional components.

- (i) First, a poor health subgroup identified by  $\mathcal{I}_\tau$  and acting on the purple path  $L_{i,k} \rightarrow A_{i,k}$  must be defined. Since a CD4 count below 500 *cells*/ $\mu L$  indicates the patients' immune system may be weakened, making them susceptible to developing serious infections from viruses, bacteria, or fungi that typically do not cause problems in healthy individuals, it is reasonable to assume that subjects in a poor health condition at visit  $k$  are identified by  $L_{i,k} < \tau$ , where  $\tau \in [0; 500]$  *cells*/ $\mu L$ . This is equivalent to a non-negative CD4 range of the form  $\mathcal{I}_\tau = [0, \tau)$ , where the upper threshold  $\tau$  has to be defined according to the simulation scenario. The higher the upper threshold  $\tau$ , the wider  $\mathcal{I}_\tau$  and the more severe the violations.
- (ii) Then, the latent individual propensity for exposure  $P_i \sim \mathcal{U}(0, 1)$  directly acts on  $A_{i,k}$ . Subjects in poor health condition with propensity  $P_i$  above the *exposure cut-off*  $\pi$  (to be defined according to the simulation scenario) are forced to start the treatment.

The procedure proposed below extends the algorithm by Havercroft and Didelez (2012) by incorporating the possibility of near-positivity violations. For details regarding the chosen parameter values, please refer to their primary work.

**Procedure** For each subject  $i = 1, \dots, n$ , the simulation procedure with  $K$  discrete time points and check-ups every  $\kappa$ -th visits is as follows.

1. Generate the individual propensity to exposure:  $P_i \sim \mathcal{U}(0, 1)$ .
2. Generate the general latent health status at baseline:  $U_{i,0} \sim \mathcal{U}(0, 1)$ .
3. Generate the baseline CD4 as a transformation of  $U_{i,0}$  by the inverse cumulative distribution function of  $\Gamma(3, 154)$  distribution plus an error  $\epsilon_{i,0} \sim \mathcal{N}(0, 20)$ :  $L_{i,0} = F_{\Gamma(3,154)}^{-1}(U_{i,0}) + \epsilon_{i,0}$ .

4. If  $P_i \geq \pi$  and  $L_{i,0} < \tau$ , the subject starts HAART and  $A_{i,0} = 1$ . Otherwise, draw treatment decision  $A_{i,0} \sim Be(p_{i,0}^A)$  where  $p_{i,0}^A = \text{logit}^{-1}[-0.405 - 0.00405 \cdot (L_{i,0} - 500)]$ . If  $A_{i,0} = 1$ , set the treatment initiation time  $K_i^*$  to 0.
5. Compute the conditional individual hazard  $\lambda_{i,0}$  for  $k = 0$  using (10). If  $\lambda_{i,0} \geq U_{i,0}$ , death has occurred in the interval  $(0, 1]$  and set  $Y_{i,1} = 1$ . Otherwise, the subject survived and set  $Y_{i,1} = 0$ .

If the individual is still at risk at visit  $k = 1$ :

6. Draw  $U_{i,k} = \min\{1, \max\{0, U_{i,k-1} + \mathcal{N}(0, 0.05)\}\}$  as a perturbation of  $U_{i,k-1}$  restricted to  $[0, 1]$ .
7. If  $k$  is not a check-up visit, CD4 cell count are not updated and  $L_{i,k} = L_{i,k-1}$ . Otherwise, update the count as  $L_{i,k} = \max\{0, L_{i,k-1} + 150 \cdot A_{i,k-1} + \epsilon_{i,k}\}$ , where the addition of 150 indicates the positive effect of exposure to HAART on CD4 count, and  $\epsilon_{i,k} \sim \mathcal{N}(100(U_{i,k} - 2), 50)$  is a Gaussian drift term implying that the worse is the general health condition  $U_{i,k}$  (i.e., value closer to 0), the stronger the negative drift in CD4.
8. If  $k$  is not a check-up visit, treatment is not updated and  $A_{i,k} = A_{i,k-1}$ . Otherwise, assign exposure
  - a. *deterministically*: if  $P_i \geq \pi$  and  $L_{i,k} < \tau$  or if treatment has started at previous check-up ( $A_{i,k-\kappa} = 1$ ), patient  $i$  is exposed to HAART and  $A_{i,k} = 1$ ;
  - b. *stochastically*: otherwise, draw treatment decision  $A_{i,k} \sim Be(p_{i,k}^A)$ , where

$$p_{i,k}^A = \text{logit}^{-1}[-0.405 + 0.0205 \cdot k - 0.00405 \cdot (L_{i,k} - 500)].$$

The conditional distribution parameters has been set to calibrate the logistic function such that  $\Pr(A_{\bullet,0} = 1 \mid L_{\bullet,0} = 500) = 0.4$ ,  $\Pr(A_{\bullet,0} = 1 \mid L_{\bullet,0} = 400) = 0.5$ , and  $\Pr(A_{\bullet,10} = 1 \mid L_{\bullet,10} = 500) = 0.45$ .

If the subject starts the treatment at visit/time  $k$ , set the treatment initiation time  $K_i^*$  equal to  $k$ .

9. Compute  $\lambda_{i,k}$ , i.e., the individual probability of failure in the interval  $(k; k+1]$  conditional on survival up to visit  $k$ , using (10). If  $S_i(t) = \prod_{j=0}^k (1 - \lambda_{i,j}) \leq 1 - U_{i,0}$ , the death has occurred in the interval  $(k; k+1]$  and  $Y_{i,k+1} = 1$ . Otherwise, the subject remains at risk and  $Y_{i,k+1} = 0$ .
10. Repeat steps 6–9 for  $k = 2, \dots, K$ .

The related pseudocode is provided in Appendix A.1. Note that when  $\pi = 1$  the positivity assumption always holds and this procedure corresponds to the data generating mechanism of Benchmark I.

## 4.2 Simulation study using Algorithm I

### 4.2.1 Methods and estimands

Investigations are performed in several scenarios by considering different sample sizes ( $n = 50, 100, 250, 500, 1000$ ), exposure cut-off values ( $\pi = 0.05, 0.1, 0.3, 0.5, 0.8, 1$ ), WT strategies (NoWT, 1-99, 5-95, 10-90), and poor health subgroups  $\mathcal{I}_\tau = [0; \tau]$  with varying upper thresholds ( $\tau = 0, 100, 200, 300, 400, 500$  measured in *cells/ $\mu$ L*). The other parameters are set to be identical to those used by [Havercroft and Didelez \(2012\)](#) to consider their results as a benchmark for this analysis. Specifically,  $K = 40$  time-points with check-ups every ( $\kappa = 5$ )-th visit are considered, and the desired conditional distribution parameters in Equation (10) are  $(\gamma_0, \gamma_{A1}, \gamma_{A2}, \gamma_{A3}) = (-3, 0.05, -1.5, 0.1)$ . In this way, the true values of the parameters in logit-MSM (9) are  $(\tilde{\gamma}_0^*, \tilde{\gamma}_{A1}^*, \tilde{\gamma}_{A2}^*, \tilde{\gamma}_{A3}^*) = (-3, 0.05, -1.5, 0.1)$ .

For each scenario,  $B = 1000$  simulated datasets are generated. The logit-MSM (9) is fitted to each simulated dataset through IPTW estimation using (truncated) stabilized weights. Weight components at time  $k$  are estimated by logistic regression models for the probability of treatment initiation at time  $k$ , with numerator and denominators in (7) defined respectively as:

$$\begin{aligned} \Pr(A_{i,k} = 1 \mid \bar{A}_{i,k-1} = \mathbf{0}, Y_{i,k-1} = 0) &= \text{logit}^{-1}[\theta_0 + \theta_1 \cdot k] \quad \text{and} \\ \Pr(A_{i,k} = 1 \mid \bar{A}_{i,k-1} = \mathbf{0}, \bar{L}_{i,k}, Y_{i,k-1} = 0) &= \text{logit}^{-1}[\theta_0 + \theta_1 \cdot k + \theta_2 \cdot (L_{i,k} - 500)]. \end{aligned}$$

In this way, since  $\pi \neq 0$ , the denominator model is correctly specified according the data-generating mechanism (Bryan, 2004; Havercroft and Didelez, 2012).

The estimands of interest are the regression coefficients  $(\tilde{\gamma}_0, \tilde{\gamma}_A)$  and the marginal survival probabilities in Equation (4) for the *always treated* versus *never treated* regimens, where  $g(\tilde{\gamma}_A; \bar{\mathbf{a}}_k) = \tilde{\gamma}_{A1} \cdot d_{1k} + \tilde{\gamma}_{A2} \cdot a_k + \tilde{\gamma}_{A3} \cdot d_{3k}$ . For each regression coefficient, estimated bias, empirical Standard Error (empSE), and Root Mean Squared Error (RMSE) (Morris et al., 2019) are considered as performance measures. Marginal survival curves are presented graphically by showing the mean estimated curves across the  $B = 1000$  repetitions.

Note that simulation settings with  $\pi = 1$  and NoWT are equivalent to Benchmark I, regardless of  $\tau$  (positivity always holds when  $\pi = 1$ ). In such cases, the analyses are based on correctly specified logit-MSMs and correctly specified models for the weights, so the resulting estimates are expected to be approximately unbiased.

#### 4.2.2 Results

The estimated performance metrics (bias, empSE, RMSE) for the regression coefficients  $(\hat{\gamma}_0, \hat{\gamma}_{A1}, \hat{\gamma}_{A2}, \hat{\gamma}_{A3})$  are provided in Supplementary Material S1. Smaller sample sizes exhibit worse performance. While increasing the sample size reduces bias and variability caused by finite sample limitations, estimation errors resulting from violations still persist, particularly for low values of  $\pi$ . Across all scenarios, as the severity of violations increases (i.e., the bigger  $\tau$  and the lower  $\pi$ ), the absolute bias, empSE, and RMSE grow substantially, particularly for  $\hat{\gamma}_0$  and  $\hat{\gamma}_{A2}$  (i.e., the intercept and the parameter most directly related to the effect of exposure). This outcome reflects how large weights resulting from near-violations increase variability and reduce precision in IPTW-based estimates. Adopting a WT strategy reduces variability and slightly decreases bias by truncating extreme weights, especially for larger  $\tau$ . However, further narrowing the truncation range (e.g., from WT 1–99 to WT 5–95 or 10–90) does not lead to additional improvements in performance; indeed, it may lead to poorer performance.

Figures 2 shows the mean marginal survival curves, along with the true ones (in orange), in each simulated scenario without WT. Each line refers to a different  $\tau$  value; the darker the line colour, the more severe the violation (i.e., the bigger  $\tau$ ). Each row refers to a different sample size ( $n = 50, 100, 250, 500, 1000$ ) and each column refers to a different exposure cut-off ( $\pi = 0.05, 0.1, 0.3, 0.5, 0.8, 1$ ). The magnitude and direction of the bias in each regression coefficient (see Supplementary Figure S1) determine how closely the estimated marginal survival curves match the true (orange) ones (see Equation (1)). Curves for *never treated* (dashed lines) depend on  $(\hat{\gamma}_0, \hat{\gamma}_{A1})$  and therefore generally show a greater deviation compared to those of *always treated* (solid lines) which depend on  $(\hat{\gamma}_0, \hat{\gamma}_{A2}, \hat{\gamma}_{A3})$ . Indeed, in the *always treated* the negative bias of  $\hat{\gamma}_0$  can be balanced by the positive one of  $\hat{\gamma}_{A2}$ . This is not true for the *never treated* so the deviation notably increases as near-positivity violations become more concrete (i.e., as  $\pi$  decreases). Similar behaviours are observed across different sample sizes as  $\pi$  varies. All scenarios eventually converged to the true values when no positivity violations are present. Contrary to what should happen, for more severe violations ( $\pi = 0.05, 0.1$ ;  $\tau = 300, 400, 500$ ), the *never treated* group demonstrates notably better survival curves compared to the *always treated* group. This deviation becomes even more pronounced with small sample sizes or when any WT strategy is applied, as illustrated in Figure 3, where each row corresponds to a different WT strategy with a sample size of  $n = 1000$ . The estimated mean curves are very close to the true ones for an expected positivity compliance rate of 80% under NoWT, or even for 50% under 1-99 WT. However, under 5-95 or 10-95 WT, estimated curves deviate from true ones, even for a high exposure cut-off.

## 5 Simulation study II

### 5.1 Data generation

The second algorithm proposed in this work is based on the data-generating mechanism introduced by Keogh et al. (2021) to simulate from an Aalen-MSM. This mechanism is now briefly introduced and then extended by imposing positivity violations.



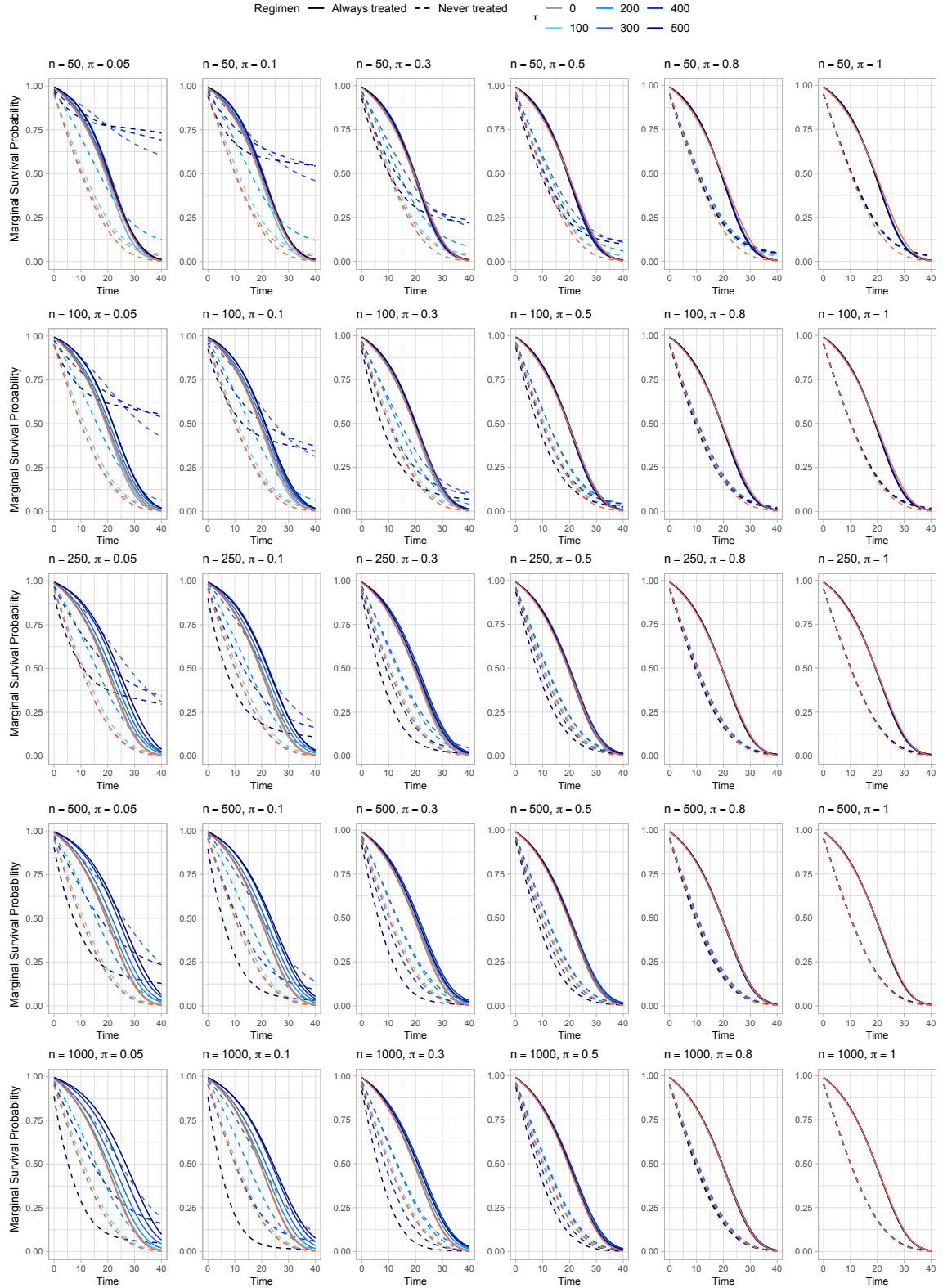


**Figure 2:** Marginal survival probability curves averaged across all the  $B = 1000$  repetitions for different settings without weight truncation (No WT) of simulation study I. Each row refers to a different sample size  $n = 50, 100, 250, 500, 1000$ . Each column refers to a different exposure cut-off  $\pi = 0.05, 0.1, 0.3, 0.5, 0.8, 1$ . Dashed lines refer to the *never treated* regimen, while solid ones to the *always treated* regimen. Curves are coloured according to different values of rule-threshold  $\tau$ . True marginal survival curves are shown in orange.

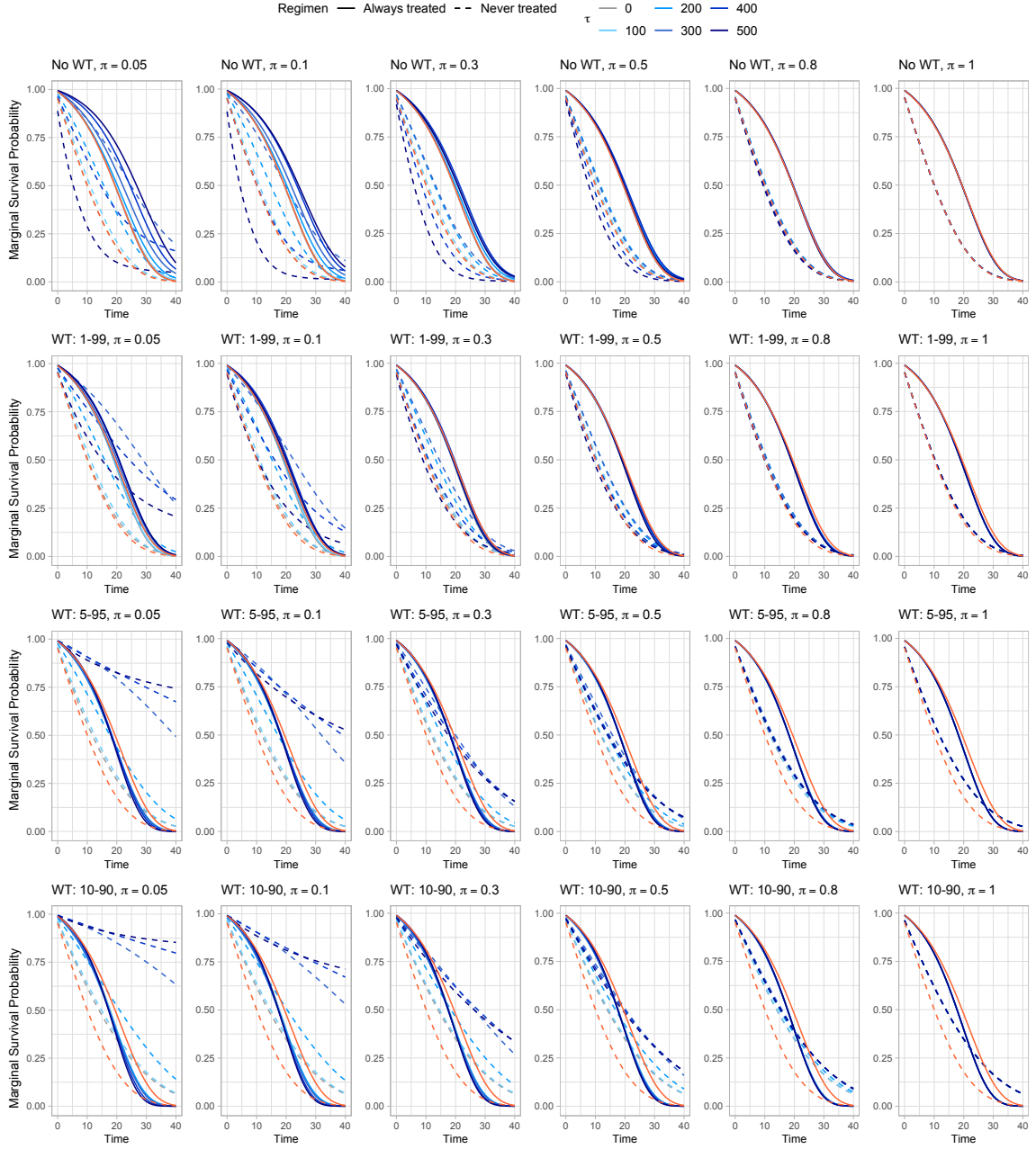


**Figure 3:** Marginal survival probability curves averaged across all the  $B = 1000$  repetitions for different settings with sample size  $n = 1000$  of simulation study I. Each row refers to a different weight truncation (WT) strategy: No WT, 1-99, 5-95, 10-99. Each column refers to a different exposure cut-off  $\pi = 0.05, 0.1, 0.3, 0.5, 0.8, 1$ . Dashed lines refer to the *never treated* regimen, while solid ones to the *always treated* regimen. Curves are coloured according to different values of rule-threshold  $\tau$ . True marginal survival curves are shown in orange.

### 5.1.1 Benchmark II in a nutshell

Keogh et al. (2021) proposed a setting where, at each visit  $k = 0, \dots, K$ , a binary treatment process  $A_{i,k} \in \{0, 1\}$  (control vs treatment) and a time-dependent biomarker  $L_{i,k} \in \mathbb{R}$  are observed for each subject  $i$ . The assumed data structure is illustrated in Figure 1b using a discrete-time DAG setting where visit times correspond to visit numbers (i.e.,  $q_k = k \forall k$ ) and  $Y_{i,k+1} = I(k < T_i \leq k + 1)$  is an indicator of whether the event  $T_i$  occurs between visits  $k$  and  $k + 1$ . As the time intervals become very small the algorithm approaches the continuous time setting. The DAG also includes a baseline latent variable  $U_i$ , representing a subject-specific unmeasured individual frailty, which has a direct effect on  $L_{i,k}$

and  $Y_{i,k+1}$ , but not on  $A_{i,k}$ .

The DAG in Figure 1b exhibits time-dependent confounding due to  $L_{i,k}$  that predicts subsequent treatment use  $A_{i,k}$ , is affected by earlier treatment  $A_{i,k-1}$ , and affects the outcome  $Y_{i,k+1}$  through pathways that are not just through subsequent treatment. Moreover, because  $U_i$  is not a confounder of the association between the treatment and the outcome, the fact that it is unmeasured does not affect the ability to estimate causal effects of treatments. The authors demonstrated that using a conditional additive hazard of the form

$$\lambda_i(t | \bar{A}_{i,[t]}, \bar{L}_{i,[t]}, U_i) = \alpha_0 + \alpha_A \cdot A_{i,[t]} + \alpha_L \cdot L_{i,[t]} + \alpha_U \cdot U_i, \quad (11)$$

their data generating mechanism correctly simulates data from the additive Aalen-MSM of the form:

$$\lambda^{\bar{a}}(t) = \tilde{\alpha}_0(t) + \sum_{j=0}^{[t]} \tilde{\alpha}_{Aj}(t) \cdot a_{[t]-j}, \quad (12)$$

that is an Aalen-MSM including as treatment-pattern  $g(\tilde{\alpha}_A(t); \bar{a}_{[t]})$  the main effect terms at each visit (see Table 1). Researchers using this approach can only specify the parameters  $(\alpha_0, \alpha_A, \alpha_L, \alpha_U)$  of the conditional model (11). The true values of the cumulative regression coefficients  $C_0(t) = \int_0^t \tilde{\alpha}_0(s)ds$  and  $C_{Aj}(t) = \int_0^t \tilde{\alpha}_{Aj}(s)ds$  ( $j = 0, \dots, 4$ ) of the Aalen-MSM (12) must be computed using a simulation-based approach, as detailed in Keogh et al. (2021).

Thanks to the collapsibility property of the Aalen’s additive hazard model, the generating mechanism of Benchmark II includes the direct arrow from  $L_{i,k}$  to  $Y_{i,k+1}$ , making it more realistic in practice compared to Benchmark I. Unlike Benchmark I, which is restricted to generating data closely matching the Swiss HIV Cohort Study (Sterne et al., 2005), Benchmark II can hence be applicable in more general contexts. However, its parameter values need to be carefully selected to ensure that the chance of obtaining a negative hazard, a common drawback in Aalen’s model, is negligible.

### 5.1.2 Algorithm II: imposing random positivity violations in Benchmark II

Analogously to Algorithm I, the second algorithm extends Benchmark II (Section 5.1.1) by imposing positivity violations randomly. As illustrated in the DAG in Figure 1d, compared to Benchmark II’s structure in Figure 1b, two components are introduced.

- (i) The latent individual propensity for exposure  $P_i \sim \mathcal{U}(0, 1)$  directly acts on  $A_{i,k}$ : subjects in poor health condition with propensity  $P_i$  above the *exposure cut-off*  $\pi$  (to be defined according to the simulation scenario) are always exposed.
- (ii) The poor health subgroup identified by  $\mathcal{I}_\tau$  acts on the purple path  $L_{i,k} \rightarrow A_{i,k}$ . In the framework of Keogh et al.’s procedure, the confounder  $L_{i,k}$  represents a general biomarker with no direct real-world interpretation, yet its higher values at time  $k$  correspond to an increased likelihood of exposure and a increased hazard. It is hence reasonable to assume that subjects with a poor health condition at time  $k$  are identified by  $L_{i,k} > \tau$ . This is equivalent to a range  $\mathcal{I}_\tau = (\tau, \infty)$ , where the lower threshold  $\tau$  has to be defined according to the simulation scenario. Here, the lower the threshold  $\tau$ , the wider the interval  $\mathcal{I}_\tau$  and the more severe the violation.

The proposed procedure extends Keogh et al.’s algorithm by incorporating the possibility for near-positivity violations. For details regarding the chosen parameter values, please refer to their primary work.

**Procedure** For each subject  $i = 1, \dots, n$ , the simulation procedure with  $K+1$  as administrative censoring time is as follows.

1. Generate the individual propensity to exposure:  $P_i \sim \mathcal{U}(0, 1)$ .
2. Generate the individual frailty term:  $U_i \sim \mathcal{N}(0, 0.1)$ .
3. Generate the baseline biomarker as a transformation of  $U_i$ :  $L_{i,0} \sim \mathcal{N}(U_i, 1)$ .
4. If  $P_i \geq \pi$  and  $L_{i,0} > \tau$ , the subject is exposed to treatment and  $A_{i,0} = 1$ . Otherwise, draw treatment decision  $A_{i,0} \sim \text{Be}(p_{i,0}^A)$  where  $p_{i,0}^A = \text{logit}^{-1}[-2 + 0.5 \cdot L_{i,0}]$ .

5. Event times in the period  $0 < t < 1$  are generated by calculating  $\Delta_i = -\log(v_{i,0})/\lambda_i(t | A_{i,0}, L_{i,0}, U_i)$ , where at numerator  $v_{i,0} \sim \mathcal{U}(0, 1)$  and the denominator is the individual conditional hazard in (11) with  $[t] = 0$  and desired parameters. If  $\Delta_i < 1$ , death occurred in the interval  $t \in (0, 1)$ : the event time is set to be  $T_i = \Delta_i$  and the failure process is  $Y_{i,1} = 1$ . Otherwise, subjects with  $\Delta_i \geq 1$  remain at risk at time  $t = 1$  and set  $Y_{i,1} = 0$ .

If the individual is still at risk at visit  $k = 1$ :

6. Update the biomarker value as:  $L_{i,k} \sim \mathcal{N}(0.8 \cdot L_{i,k-1} - A_{i,k-1} + 0.1 \cdot k + U_i, 1)$ .
7. Assign exposure
  - a. *deterministically*: if  $P_i \geq \pi$  and  $L_{i,k} > \tau$ , subject  $i$  is exposed to treatment and  $A_{i,k} = 1$ ;
  - b. *stochastically*: otherwise, draw treatment decision  $A_{i,k} \sim \text{Be}(p_{i,k}^A)$  where

$$p_{i,k}^A = \text{logit}^{-1}[-2 + 0.5 \cdot L_{i,k} + A_{i,k}].$$

8. Event times in the period  $k \leq t < k + 1$  are generated by calculating  $\Delta_i = -\frac{\log(v_{i,k})}{\lambda_i(t | \bar{A}_{i,k}, \bar{L}_{i,k}, U_i)}$ , where  $v_{i,k} \sim \mathcal{U}(0, 1)$  and the denominator is the individual conditional hazard in (11) with  $[t] = k$  and desired parameters. If  $\Delta_i < 1$ , death occurred in the interval  $[k, k + 1)$ : the event time is set to be  $T_i = k + \Delta_i$  and the failure process is  $Y_{i,k+1} = 1$ . Otherwise, subjects with  $\Delta_i \geq 1$  remain at risk at time  $k + 1$ , i.e.,  $Y_{i,k+1} = 0$ .
9. Repeat steps 6-8 for  $k = 2, \dots, K$ . Subjects who do not have an event time generated in the period  $0 < t < K + 1$  are administratively censored at time  $K + 1$ .

The related pseudocode is provided in Appendix A.2. Note that when  $\pi = 1$  the positivity assumption always holds and this procedure corresponds to the data generating mechanism of Benchmark II.

## 5.2 Simulation study using Algorithm II

### 5.2.1 Methods and estimands

Investigations are performed in several scenarios by considering different sample sizes ( $n = 50, 100, 250, 500, 1000$ ), exposure cut-off values ( $\pi = 0, 0.05, 0.1, 0.3, 0.5, 0.8, 1$ ), WT strategies (NoWT, 1-99, 5-95, 10-90), and poor health subgroups identified by intervals  $\mathcal{I}_\tau = (\tau; \infty)$  with varying lower threshold  $\tau$ . Since  $L_{i,k}$  represents a general biomarker with no direct real-world interpretation, the choice of possible values for  $\tau$  relies on the distribution of the complete history of biomarker values generated using Benchmark II with 100,000 subjects. Specifically, the rounded values closest to the 80th, 90th, 95th, 99th, and 100th percentiles (i.e.,  $\tau = 1, 1.5, 2, 3, 7$ ) plus an extreme value outside the observed range (i.e.,  $\tau = 10$ ) are considered as possible lower thresholds. The other parameters are set to be identical to those considered by Keogh et al. (2021) in order to (i) have the same true values of the estimands of interest for the Aalen-MSM (12) (see Tables 1 and 2 in Keogh et al. (2021)), (ii) use their results as a benchmark for this analysis, and (iii) ensure that the probability of obtaining a negative hazard is negligible for Benchmark II. Specifically,  $K = 4$  time-points with administrative censoring at  $K + 1$  are considered, and the conditional distribution parameters in Equation (11) were  $(\alpha_0, \alpha_A, \alpha_L, \alpha_U) = (0.7, -0.2, 0.05, 0.05)$ .

For each scenario,  $B = 1000$  simulated datasets are generated. The Aalen-MSM (12) is fitted to each simulated dataset through IPTW estimation using (truncated) stabilized weights. Weight components at time  $k$  are estimated by logistic regression models for the probability of being exposed at time  $k$ , with numerator and denominators in (7) defined respectively as:

$$\begin{aligned} \Pr(A_{i,k} = 1 | \bar{A}_{i,k-1}, T_i \geq k) &= \text{logit}^{-1}[\theta_0 + \theta_1 \cdot A_{i,k-1}] \quad \text{and} \\ \Pr(A_{i,k} = 1 | \bar{A}_{i,k-1}, \bar{L}_{i,k}, T_i \geq k) &= \text{logit}^{-1}[\theta_0 + \theta_1 \cdot A_{i,k-1} + \theta_2 \cdot L_{i,k}]. \end{aligned}$$

In this way, since  $\pi \neq 0$ , the denominator model is correctly specified according the data generation mechanism (Keogh et al., 2021).

The estimands of interest are the cumulative regression coefficients  $C_0(t) = \int_0^t \tilde{\alpha}_0(s)ds$  and  $C_{A_j}(t) = \int_0^t \tilde{\alpha}_{A_j}(s)ds$  ( $j = 0, \dots, 4$ ), and the marginal survival probabilities in Equation (6) for the *always treated*

and *never treated* regimens, where  $g(\tilde{\alpha}_A(t); \bar{a}_{[t]}) = \sum_{j=0}^{\lfloor t \rfloor} \tilde{\alpha}_{Aj}(t) \cdot a_{[t]-j}$ . For the cumulative regression coefficients, results are presented graphically by showing the performance (i.e., bias, empSE, and RMSE) measured at times  $t = 1, 2, 3, 4, 5$ . For the marginal survival curves, the mean value of the estimates across repetitions are presented graphically across time points  $t = 1, 2, 3, 4, 5$ .

Note that simulation settings with  $\pi = 1$  and NoWT are equivalent to Benchmark II, regardless of  $\tau$  (positivity always holds). In such cases, the analyses are based on correctly specified Aalen-MSMs and correctly specified models for the weights, so the resulting estimates are expected to be approximately unbiased.

## 5.2.2 Results

The performance metrics for the estimated cumulative coefficients over time  $t = 1, 2, 3, 4, 5$  in each simulated scenario are provided in Supplementary Material S2. For cumulative coefficient  $\hat{C}_{A0}(t)$  related to the current main effect terms, smaller sample sizes exhibit worse performance, as increasing the sample size only mitigates the bias induced by finite sample issues. Across scenarios, bias, empSE, and RMSE increase with time. In general, the more severe the violation (i.e., low  $\pi$ , low  $\tau$ ), the higher empSE and RMSE. Adopting a WT strategy decreases empSE and RMSE, as extreme weights are truncated, especially for more severe violations. However, compared to WT 1-99, narrowing down the WT resulted in worse bias over time. Results eventually converge to be unbiased under NoWT, but a small bias still persists under 1-99 WT for  $t = 4, 5$ . In terms of variability, the empSE are comparable to the one estimated in Benchmark II, even when the expected positivity non-compliance rate is 80%. Results for the other cumulative coefficients led to similar conclusions: (i) the performance worsen with time; (ii) adopting a WT strategy reduces the variability; (ii) estimated performance eventually converge to the ones estimated for the Benchmark II. The estimated bias for  $\hat{C}_0(t)$ , i.e., the cumulative intercept, is negative, and decreases with time (see Supplementary Figure S4). For large sample sizes ( $n = 500, 1000$ ), the difference in the bias across  $\pi$  values is minimal. The other treatment-related coefficients  $\hat{C}_{Aj}(t)$  with  $j = 1, 2, 3, 4$  exhibit higher empSE and RMSE as the violation severity increases. Unlike  $\hat{C}_{A0}(t)$ , however, no discernible relationship was found between the values of  $\tau$  and the resulting bias.

Figure 4 shows the mean marginal survival curves over times  $t = 1, 2, 3, 4, 5$  across repetitions estimated in the various scenarios without WT, along with the true ones (in green). Each line refers to a different  $\tau$  value; the darker the line colour, the more severe the violation (i.e., the smaller  $\tau$ ). Each row refers to a different sample size ( $n = 50, 100, 250, 500, 1000$ ) and each column to a different exposure cut-off ( $\pi = 0.05, 0.1, 0.3, 0.5, 0.8, 1$ ). These curves can be derived from the cumulative coefficients – as in Equation (6) – whose estimates determine how closely the estimated mean curves match the true (green) ones. At each time point  $t = 1, 2, 3, 4, 5$ , the curves for *never treated* (dashed lines) depend solely on  $\hat{C}_0(t)$ , while all cumulative coefficients contribute to estimating the curves for *always treated* (solid lines). As a result, the estimated mean curves for *never treated* align with the true (green) curves for big sample sizes, exhibiting very low bias across time points. Conversely, summing the contributions of each cumulative coefficients leads to higher bias for the *always treated*, especially at later time points. Small sample sizes heavily suffer from the main drawback of the additive hazard model, which does not restrict the hazard to be non-negative. This determines survival probabilities for the *always treated* that wrongly increase over time. This issue is mitigated for bigger samples sizes ( $n = 500, 1000$ ). As the exposure cut-off  $\pi$  increases, the estimated mean curves correspond to the true ones for an expected positivity compliance rate from 80% upwards under NoWT, or even from 30% under 1-99 WT. Adopting 1-99 WT (see Figure 5) improves the performance compared to NoWT. Nonetheless, compared to WT 1-99, narrowing down the WT resulted in worse bias over time.

## 6 Discussion

Simulation studies play a key role in evaluating robustness to assumption violations, enabling the examination of various properties (Morris et al., 2019; Friedrich and Friede, 2023). While existing literature on positivity violations in MSMs has largely focused on incorrect inferences using real data or simulations with exposure assigned at a single or two time points, this study fills the gap by presenting two simulation studies in realistic survival contexts involving a time-varying binary treatment and a continuous time-dependent confounder. Two distinct algorithms were proposed to simulate data from hazard-MSMs and to account for potential near-positivity violations, where remaining unexposed is rare within certain

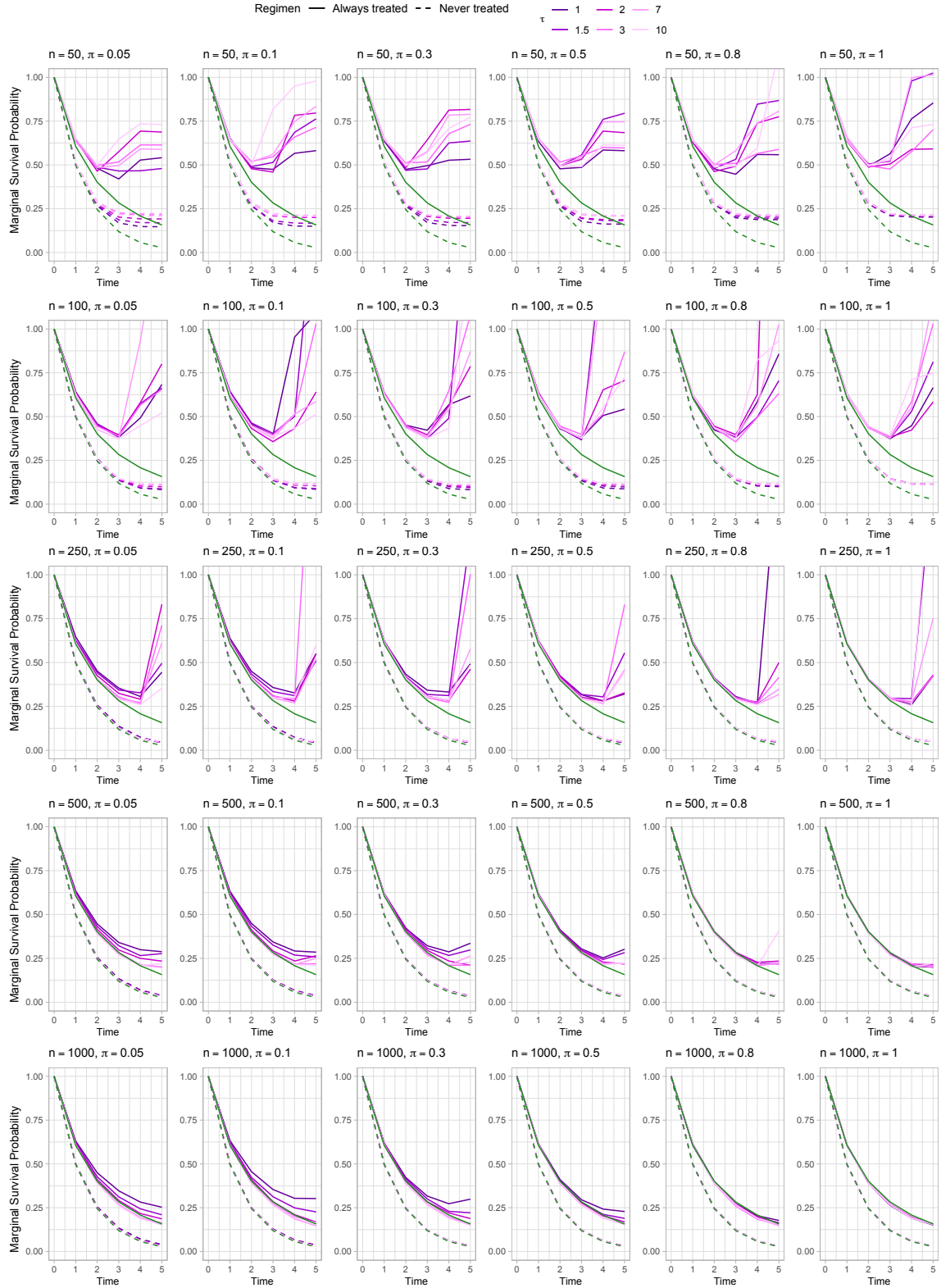


**Figure 4:** Marginal survival probability curves averaged across all the  $B = 1000$  repetitions for different settings without weight truncation (No WT) of simulation study II. Each row refers to a different sample size  $n = 50, 100, 250, 500, 1000$ . Each column refers to a different exposure cut-off  $\pi = 0.05, 0.1, 0.3, 0.5, 0.8, 1$ . Dashed lines refer to the *never treated* regimen, while solid ones to the *always treated* regimen. Curves are coloured according to different values of rule-threshold  $\tau$ . True marginal survival curves are shown in green.



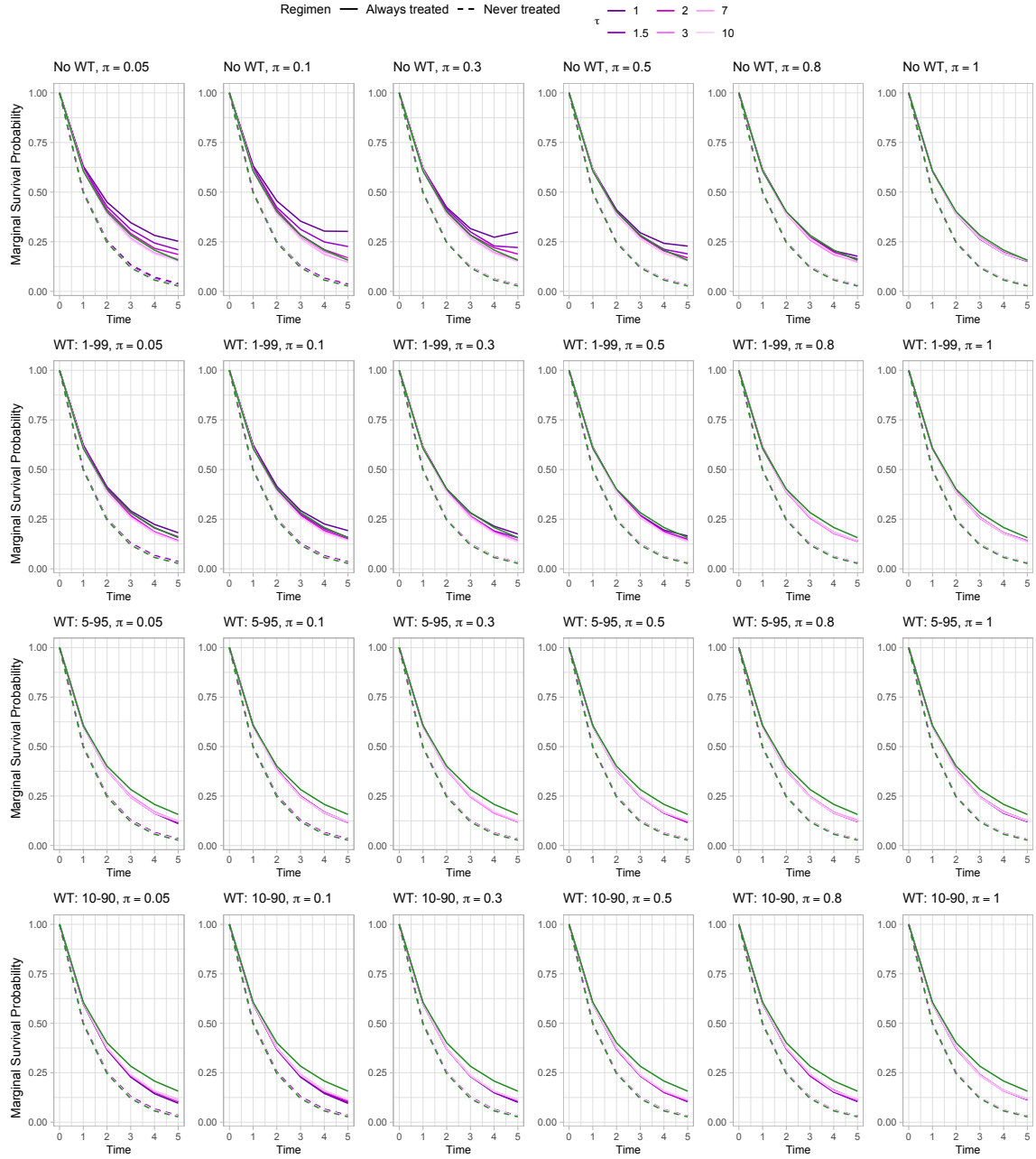


**Figure 5:** Marginal survival probability curves averaged across all the  $B = 1000$  repetitions for different settings with sample size  $n = 1000$  of simulation study II. Each row refers to a different weight truncation (WT) strategy: No WT, 1-99, 5-95, 10-99. Each column refers to a different exposure cut-off  $\pi = 0.05, 0.1, 0.3, 0.5, 0.8, 1$ . Dashed lines refer to the *never treated* regimen, while solid ones to the *always treated* regimen. Curves are coloured according to different values of rule-threshold  $\tau$ . True marginal survival curves are shown in green.

confounder levels. Systematic simulations were conducted to evaluate the impact of near-positivity violations on the performance of target estimands obtained via IPTW under various scenarios and WT strategies.

Findings from both studies revealed a consistent trend: as the violation becomes more severe (i.e., low  $\pi$ ), performance deteriorates. Increasing the sample size mitigates bias and variability due to finite sample size, but incorrect inference resulting from positivity violations persists. Even when  $\mathcal{I}_\tau$  is small, performance may still be poor due to the presence of extreme weights. Under NoWT, the higher the positivity compliance rate, the better the performance aligns with Benchmark I and II. Adopting a WT strategy always reduces variability by truncating extreme weights, especially for wider  $\mathcal{I}_\tau$ . However,

compared to WT 1-99, narrowing down the WT may not improve bias. This suggests that bias becomes the more dominant factor when the positivity assumption is violated. The decision to adopt the 1-99 WT strategy in cases of near-violations should carefully consider the bias-variance trade-off. For intermediate positivity compliance rates ( $\pi = 0.3, 0.5$ ), the 1-99 WT strategy generally outperformed NoWT. In contrast, for high values ( $\pi = 0.8, 1$ ), NoWT was more effective.

Algorithm I and II proposed in this work were built on prior algorithms by [Havercroft and Didelez \(2012\)](#) and [Keogh et al. \(2021\)](#), respectively. The advantage of extending existing algorithms was three-fold. First, the issue of non-collapsibility ([Robinson and Jewell, 1991](#); [Didelez and Stensrud, 2022](#)) between conditional and marginal models and the replication of complex confounding dynamics have been already overcome in the original studies. Second, by controlling the exposure-confounder path and avoiding misspecification of the weighting model, the effect due to the imposed positivity violations was separated from other sources of bias. Third, the original Benchmarks I and II were used as the references for the expected true estimates when positivity is valid (i.e., for  $\pi = 1$ ).

While a direct comparison is not feasible as they pertain to different data-generating mechanisms, Algorithm I generally exhibited poorer performance compared to Algorithm II. This difference may stem from their distinct treatment decision mechanisms. Algorithm I requires continuous exposure until failure or censoring once treatment begins, whereas Algorithm II does not have such a requirement. This constraint limits the possible combinations of treatment-covariate history in Algorithm I, with a significant impact on the estimated coefficients even though very few combinations are missing. Consequently, this influences the estimated mean survival curves, leading to incorrect survival probabilities for the *never treated* group. On the other hand, Algorithm II suffers, especially with small sample sizes, from the linear form of the Aalen-MSM, which does not restrict the hazard to be non-negative, resulting in unrealistic survival estimates.

This work has its limitations, which also open up intriguing possibilities for future research. Both studies focused on instances where violations occur within a single interval of the confounder variable and examined only a single continuous confounding variable. However, in real-world scenarios, violations may span varied intervals, and multiple continuous/categorical confounding factors are typically present. This highlights interesting directions for extending the proposed algorithms, though adapting them to new contexts will require meticulous adjustments. Nonetheless, in their current form, Algorithms I and II developed in this study represent a valuable contribution to the literature. They could serve as data-generating tools for systematic analyses, enabling for (i) the comparison of different techniques for estimating causal effects from observational data under near-positivity violations and (ii) the evaluation of potential new methods designed to address near-positivity violations in a longitudinal-treatment framework. Since current methods for detecting and addressing positivity violations are primarily tailored to point-treatment settings ([Traskin and Small, 2011](#); [Karavani et al., 2019](#); [Zhu et al., 2023](#); [Danelian et al., 2023](#); [Zivich et al., 2024](#)), developing methodologies specifically suited to a longitudinal framework presents a challenging direction for future research.

In summary, this study emphasizes the importance of carefully assessing positivity compliance to ensure robust and reliable causal inference in survival studies, while also highlighting the risks of underestimating it. By demonstrating the substantial impact of near-positivity violations, it underscores the need for rigour in causal inference, particularly given the exponential growth of causal inference approaches and their applications to observational data. In practical analyses, researchers are strongly encouraged to examine group-wise descriptives for the original and weighted populations, utilize bootstrap to quantify uncertainty in weights, and conduct sensitivity analysis for further insights ([Cole and Hernán, 2008](#); [Austin and Stuart, 2015](#); [Desai and Franklin, 2019](#)). The causal effect of interest must be defined with consideration of positivity violations. While adopting a WT strategy may reduce variability, it should be approached with caution due to the potential risk of increased bias. Although IPTW-based MSMs are widely used in applied studies for their simplicity in implementation and interpretation, analysts must remain vigilant about blindly accepting the positivity assumption, as doing so can lead to detrimental consequences. Finally, the two algorithms developed in this study also serve as valuable tools for generating data in future systematic analyses of novel causal inference methodologies.

**Acknowledgments.** The author would like to thank Prof.dr. Marta Fiocco (Mathematical Institute, Leiden University) for constructive discussions on the current work.

## References

- Austin, P. C. and Stuart, E. A. (2015). Moving towards best practice when using inverse probability of treatment weighting (IPTW) using the propensity score to estimate causal treatment effects in observational studies. *Stat. Med.*, 34(28):3661–3679.
- Bembom, O. and van der Laan, M. J. (2007). A practical illustration of the importance of realistic individualized treatment rules in causal inference. *Electron. J. Stat.*, 1:574–596.
- Bryan, J. (2004). Analysis of longitudinal marginal structural models. *Biostat.*, 5(3):361–380.
- Clare, P. J., Dobbins, T. A., and Mattick, R. P. (2019). Causal models adjusting for time-varying confounding—a systematic review of the literature. *Int. J. Epidemiol.*, 48(1):254–265.
- Cole, S. R. and Frangakis, C. E. (2009). The Consistency Statement in Causal Inference. *Epidemiol.*, 20(3-5).
- Cole, S. R. and Hernán, M. A. (2008). Constructing Inverse Probability Weights for Marginal Structural Models. *Am. J. Epidemiol.*, 168(6):656–664.
- Danelian, G., Foucher, Y., Léger, M., Le Borgne, F., and Chatton, A. (2023). Identification of in-sample positivity violations using regression trees: The PoRT algorithm. *J. Causal Inference*, 11(1).
- Daniel, R. M., Cousens, S. N., De Stavola, B. L., Kenward, M. G., and Sterne, J. A. (2013). Methods for dealing with time-dependent confounding. *Stat. Med.*, 32(9):1584–1618.
- Desai, R. J. and Franklin, J. M. (2019). Alternative approaches for confounding adjustment in observational studies using weighting based on the propensity score: a primer for practitioners. *BMJ*, 367:l5657.
- Didelez, V. and Stensrud, M. J. (2022). On the logic of collapsibility for causal effect measures. *Biom. J.*, 64(2):235–242.
- Evans, R. J. and Didelez, V. (2023). Parameterizing and simulating from causal models. *J. R. Stat. Soc. Series B Stat. Methodol.*, qkad058.
- Feuerriegel, S., Frauen, D., Melnychuk, V., Schweisthal, J., Hess, K., Curth, A., Bauer, S., Kilbertus, N., Kohane, I. S., and van der Schaar, M. (2024). Causal machine learning for predicting treatment outcomes. *Nat. Med.*, 30(4):958–968.
- Friedrich, S. and Friede, T. (2023). On the role of benchmarking data sets and simulations in method comparison studies. *Biom. J.*, page e2200212.
- Gabriel, E. E., Sachs, M. C., Waernbaum, I., Goetghebuer, E., Blanche, P. F., Vansteelandt, S., Sjölander, A., and Scheike, T. (2024). Propensity weighting plus adjustment in proportional hazards model is not doubly robust. *Biometrics*, 80(3).
- Hammerton, G. and Munafò, M. R. (2021). Causal inference with observational data: the need for triangulation of evidence. *Psychol. Med.*, 51(4):563–578.
- Havercroft, W. G. and Didelez, V. (2012). Simulating from marginal structural models with time-dependent confounding. *Stat. Med.*, 31(30):4190–4206.
- Hernán, M. and Robins, J. (2020). *Causal Inference: What If*. Boca Raton: Chapman & Hall/CRC.
- Hernán, M. A. (2010). The hazards of hazard ratios. *Epidemiology*, 21(1):13–15.
- Hernán, M. A., Brumback, B., and Robins, J. M. (2000). Marginal structural models to estimate the causal effect of zidovudine on the survival of HIV-positive men. *Epidemiol.*, 11(5):561–570.
- Hernán, M. A. and Robins, J. M. (2016). Using big data to emulate a target trial when a randomized trial is not available. *Am. J. Epidemiol.*, 183(8):758–764.
- Hernán, M. A. (2021). Methods of Public Health Research - Strengthening Causal Inference from Observational Data. *N. Engl. J. Med.*, 385(15):1345–1348.
- Karavani, E., Bak, P., and Shimon, Y. (2019). A discriminative approach for finding and characterizing positivity violations using decision trees. *arXiv*, 1907.08127.

- Keogh, R. H., Seaman, S. R., Gran, J. M., and Vansteelandt, S. (2021). Simulating longitudinal data from marginal structural models using the additive hazard model. *Biom. J.*, 63(7):1526–1541.
- Keogh, R. H. and van Geloven, N. (2024). Prediction under interventions: Evaluation of counterfactual performance using longitudinal observational data. *Epidemiology*, 35(3):329–339.
- Léger, M., Chatton, A., Le Borgne, F., Pirracchio, R., Lasocki, S., and Foucher, Y. (2022). Causal inference in case of near-violation of positivity: comparison of methods. *Biom. J.*, 64(8):1389–1403.
- Lin, L., Sperrin, M., Jenkins, D. A., Martin, G. P., and Peek, N. (2021). A scoping review of causal methods enabling predictions under hypothetical interventions. *Diagn. Progn. Res.*, 5(1):3.
- Martinussen, T., Vansteelandt, S., and Andersen, P. K. (2020). Subtleties in the interpretation of hazard contrasts. *Lifetime Data Anal.*, 26(4):833–855.
- Mitra, N., Roy, J., and Small, D. (2022). The future of causal inference. *Am. J. Epidemiol.*, 191(10):1671–1676.
- Moccia, C., Moirano, G., Popovic, M., Pizzi, C., Fariselli, P., Richiardi, L., Ekstrøm, C. T., and Maule, M. (2024). Machine learning in causal inference for epidemiology. *Eur. J. Epidemiol.*, 39(10):1097–1108.
- Morris, T. P., White, I. R., and Crowther, M. J. (2019). Using simulation studies to evaluate statistical methods. *Stat. Med.*, 38(11):2074–2102.
- Mortimer, K. M., Neugebauer, R., van der Laan, M., and Tager, I. B. (2005). An application of model-fitting procedures for marginal structural models. *Am. J. Epidemiol.*, 162(4):382–388.
- Naimi, A. I., Cole, S. R., Westreich, D. J., and Richardson, D. B. (2011). A comparison of methods to estimate the hazard ratio under conditions of time-varying confounding and nonpositivity. *Epidemiol.*, 22(5):718–723.
- Neugebauer, R. and van der Laan, M. J. (2005). Why prefer double robust estimators in causal inference? *J. Stat. Plan. Inference*, 129(1-2):405–426.
- Olier, I., Zhan, Y., Liang, X., and Volovici, V. (2023). Causal inference and observational data. *BMC Med. Res. Methodol.*, 23(227).
- Petersen, M. L., Porter, K. E., Gruber, S., Wang, Y., and van der Laan, M. J. (2012). Diagnosing and responding to violations in the positivity assumption. *Stat. Methods Med. Res.*, 21(1):31–54.
- R Core Team (2023). *R: A Language and Environment for Statistical Computing*. R Foundation for Statistical Computing, Vienna, Austria.
- Robins, J. M., Blevins, D., Ritter, G., and Wulfsohn, M. (1992). G-estimation of the effect of prophylaxis therapy for *Pneumocystis carinii* pneumonia on the survival of AIDS patients. *Epidemiol.*, 3(4):319–336.
- Robins, J. M., Hernán, M. A., and Brumback, B. (2000). Marginal structural models and causal inference in epidemiology. *Epidemiol.*, 11(5):550–560.
- Robinson, L. D. and Jewell, N. P. (1991). Some surprising results about covariate adjustment in logistic regression models. *Int. Stat. Rev.*, 59(2):227.
- Rudolph, J. E., Benkeser, D., Kennedy, E. H., Schisterman, E. F., and Naimi, A. I. (2022). Estimation of the average causal effect in longitudinal data with time-varying exposures: The challenge of nonpositivity and the impact of model flexibility. *Am. J. Epidemiol.*, 191(11):1962–1969.
- Seaman, S. R. and Keogh, R. H. (2024). Simulating data from marginal structural models for a survival time outcome. *Biom. J.*, 66(8):e70010.
- Sterne, J. A. C., Hernán, M. A., Ledergerber, B., Tilling, K., Weber, R., Sendi, P., Rickenbach, M., Robins, J. M., Egger, M., and Swiss HIV Cohort Study (2005). Long-term effectiveness of potent antiretroviral therapy in preventing AIDS and death: a prospective cohort study. *Lancet*, 366(9483):378–384.
- Traskin, M. and Small, D. S. (2011). Defining the study population for an observational study to ensure sufficient overlap: A tree approach. *Stat. Biosci.*, 3(1):94–118.
- van der Laan, M. and Gruber, S. (2016). One-step targeted minimum loss-based estimation based on universal least favorable one-dimensional submodels. *Int. J. Biostat.*, 12(1):351–378.

- van Geloven, N., Swanson, S. A., Ramspek, C. L., Luijken, K., van Diepen, M., Morris, T. P., Groenwold, R. H. H., van Houwelingen, H. C., Putter, H., and le Cessie, S. (2020). Prediction meets causal inference: the role of treatment in clinical prediction models. *Eur. J. Epidemiol.*, 35(7):619–630.
- Wang, Y., Petersen, M., Bangsberg, D., and van der Laan, M. J. (2006). Diagnosing bias in the inverse probability of treatment weighted estimator resulting from violation of experimental treatment assignment. *U.C. Berkeley Division of Biostatistics Working Paper Series*, Working Paper 211.
- Williamson, T. and Ravani, P. (2017). Marginal structural models in clinical research: when and how to use them? *Nephrol. Dial. Transplant.*, 32(suppl 2):ii84–ii90.
- Xiao, Y., Abrahamowicz, M., and Moodie, E. E. M. (2010). Accuracy of conventional and marginal structural Cox model estimators: a simulation study. *Int. J. Biostat.*, 6(2):Article 13.
- Xiao, Y., Moodie, E. E. M., and Abrahamowicz, M. (2013). Comparison of approaches to weight truncation for marginal structural Cox models. *Epidemiol. Method.*, 2(1):1–20.
- Young, J. G., Hernán, M. A., Picciotto, S., and Robins, J. M. (2010). Relation between three classes of structural models for the effect of a time-varying exposure on survival. *Lifetime Data Anal.*, 16(1):71–84.
- Young, J. G. and Tchetgen Tchetgen, E. J. (2014). Simulation from a known Cox MSM using standard parametric models for the g-formula. *Stat. Med.*, 33(6):1001–1014.
- Zhu, A. Y., Mitra, N., and Roy, J. (2023). Addressing positivity violations in causal effect estimation using gaussian process priors. *Stat. Med.*, 42(1):33–51.
- Zhu, Y., Hubbard, R. A., Chubak, J., Roy, J., and Mitra, N. (2021). Core concepts in pharmacoepidemiology: Violations of the positivity assumption in the causal analysis of observational data: Consequences and statistical approaches. *Pharmacoepidemiol. Drug Saf.*, 30(11):1471–1485.
- Zivich, P. N., Edwards, J. K., Lofgren, E. T., Cole, S. R., Shook-Sa, B. E., and Lessler, J. (2024). Transportability without positivity: A synthesis of statistical and simulation modeling. *Epidemiology*, 35(1):23–31.

# Appendix

## A.1 Pseudocode of Algorithm I

---

**Algorithm I** Pseudocode of Algorithm I introduced in Section ??.

---

**Input parameters:**

$n$  = sample size,  $\tau$  = rule-threshold,  $\pi$  = compliance threshold

$K$  = number of visits,  $\kappa$  = check-up times,

$(\gamma_0, \gamma_{A1}, \gamma_{A2}, \gamma_{A3})$  = conditional distribution parameters in Equation (10)

---

**Algorithm:**

**for** each subject  $i = 1, \dots, n$  **do**

$P_i \sim \mathcal{U}(0, 1)$

▷ Individual propensity

$U_{i,0} \sim \mathcal{U}(0, 1)$

$L_{i,0} = F_{\Gamma(3,154)}^{-1}(U_{i,0}) + \epsilon_{i,0}$  where  $\epsilon_{i,0} \sim \mathcal{N}(0, 20)$

**if**  $P_i \geq \pi$  and  $L_{i,0} < \tau$  **then**

$A_{i,0} = 1$

▷ Deterministic exposure assignment

**else**

$p_{i,0}^A = \text{logit}^{-1}[-0.405 - 0.00405 \cdot (L_{i,0} - 500)]$

▷ Stochastic exposure assignment

$A_{i,0} \sim \text{Be}(p_{i,0}^A)$

**end if**

**if**  $A_{i,0} = 1$  **then**  $K_i^* = 0$

**end if**

$\lambda_{i,0} = \text{logit}^{-1}[\gamma_{A0} + \gamma_{A2} \cdot A_{i,0}]$

▷ Conditional hazard (10)

**if**  $\lambda_{i,0} \geq U_{i,0}$  **then**  $Y_{i,1} = 1$

**else**  $Y_{i,1} = 0$

**end if**

$k = 1$

**while**  $Y_{i,k} = 0$  and  $k \leq K$  **do**

$U_{i,k} = \min\{1, \max\{0, U_{i,k-1} + \epsilon_{i,k}\}\}$  where  $\epsilon_{i,k} \sim \mathcal{N}(0, 0.05)$

**if**  $k \bmod \kappa \neq 0$  **then**

$L_{i,k} = L_{i,k-1}$

$A_{i,k} = A_{i,k-1}$

**else**

$L_{i,k} = \max\{0, L_{i,k-1} + 150 \cdot A_{i,k-1} + \epsilon_{i,k}\}$  where  $\epsilon_{i,k} \sim \mathcal{N}(100(U_{i,k} - 2), 50)$

**if**  $(P_i \geq \pi$  and  $L_{i,k} < \tau)$  or  $A_{i,k-\kappa} = 1$  **then**

$A_{i,k} = 1$

▷ Deterministic exposure assignment

**else**

$p_{i,k}^A = \text{logit}^{-1}[-0.405 + 0.0205 \cdot k - 0.00405 \cdot (L_{i,k} - 500)]$

▷ Stochastic exposure assignment

$A_{i,k} \sim \text{Be}(p_{i,k}^A)$

**end if**

**if**  $A_{i,k} = 1$  and  $A_{i,k-1} = 0$  **then**  $K_i^* = k$

**end if**

**end if**

▷ Conditional hazard (10)

$\lambda_{i,k} = \text{logit}^{-1}[\gamma_0 + \gamma_{A1} \cdot \{(1 - A_{i,k})k + A_{i,k}K_i^*\} + \gamma_{A2} \cdot A_{i,k} + \gamma_{A3} \cdot A_{i,k}(k - K_i^*)]$

**if**  $\prod_{j=0}^k (1 - \lambda_{i,j}) \leq 1 - U_{i,0}$  **then**  $Y_{i,k+1} = 1$

**else**  $Y_{i,k+1} = 0$

**end if**

$k = k + 1$

**end while**

**end for**

---



## A.2 Pseudocode of Algorithm II

---

**Algorithm II** Pseudocode of Algorithm II introduced in Section ??.

---

**Input parameters:**

$n$  = sample size,  $\tau$  = rule-threshold,  $\pi$  = compliance threshold,

$K$  = number of visits,  $(\alpha_0, \alpha_A, \alpha_L, \alpha_U)$  = desired true parameters in Equation 11

---

**Algorithm:**

**for** each subject  $i = 1, \dots, n$  **do**

$P_i \sim \mathcal{U}(0, 1)$

▷ Individual propensity

$U_{i,0} \sim \mathcal{N}(0, 1)$

$L_{i,0} \sim \mathcal{N}(U_i, 1)$

**if**  $P_i \geq \pi$  and  $L_{i,0} > \tau$  **then**

$A_{i,0} = 1$

▷ Deterministic exposure assignment

**else**

$p_{i,0}^A = \text{logit}^{-1}[-2 + 0.5 \cdot L_{i,0}]$

▷ Stochastic exposure assignment

$A_{i,0} \sim \text{Be}(p_{i,0}^A)$

**end if**

$\lambda_i(t \mid A_{i,0}, L_{i,0}, U_i) = \alpha_0 + \alpha_A \cdot A_{i,0} + \alpha_L \cdot L_{i,0} + \alpha_U \cdot U_i$

▷ Conditional hazard (11)

$\Delta_i = -\log(v_{i,0})/\lambda_i(t \mid A_{i,0}, L_{i,0}, U_i)$  where  $v_{i,0} \sim \mathcal{U}(0, 1)$

**if**  $\Delta_i < 1$  **then**  $T_i = \Delta_i$  and  $Y_{i,1} = 1$

**else**  $Y_{i,1} = 0$

**end if**

$k = 1$

**while**  $Y_{i,k} = 0$  and  $k \leq K$  **do**

$L_{i,k} \sim \mathcal{N}(0.8 \cdot L_{i,k-1} - A_{i,k-1} + 0.1 \cdot k + U_i, 1)$

**if**  $P_i \geq \pi$  and  $L_{i,k} > \tau$  **then**

$A_{i,k} = 1$

▷ Deterministic exposure assignment

**else**

$p_{i,k}^A = \text{logit}^{-1}[-2 + 0.5 \cdot L_{i,k} + A_{i,k}]$

▷ Stochastic exposure assignment

$A_{i,k} \sim \text{Be}(p_{i,k}^A)$

**end if**

$\lambda_i(t \mid \bar{A}_{i,k}, \bar{L}_{i,k}, U_i) = \alpha_0 + \alpha_A \cdot A_{i,k} + \alpha_L \cdot L_{i,k} + \alpha_U \cdot U_i$

▷ Conditional hazard (11)

$\Delta_i = -\log(v_{i,k})/\lambda_i(t \mid A_{i,0}, L_{i,0}, U_i)$  where  $v_{i,k} \sim \mathcal{U}(0, 1)$

**if**  $\Delta_i < 1$  **then**  $T_i = k + \Delta_i$  and  $Y_{i,k+1} = 1$

**else**  $Y_{i,k+1} = 0$

**end if**

$k = k + 1$

**end while**

**if**  $\text{is.null}(T_i)$  **then**  $T_i = K + 1$

**end if**

▷ Administrative censoring at  $K + 1$

**end for**

---

# Supplementary Material

## S1 Simulation study I: additional results

Bias for estimated regression coefficients of logit-MSM (9)

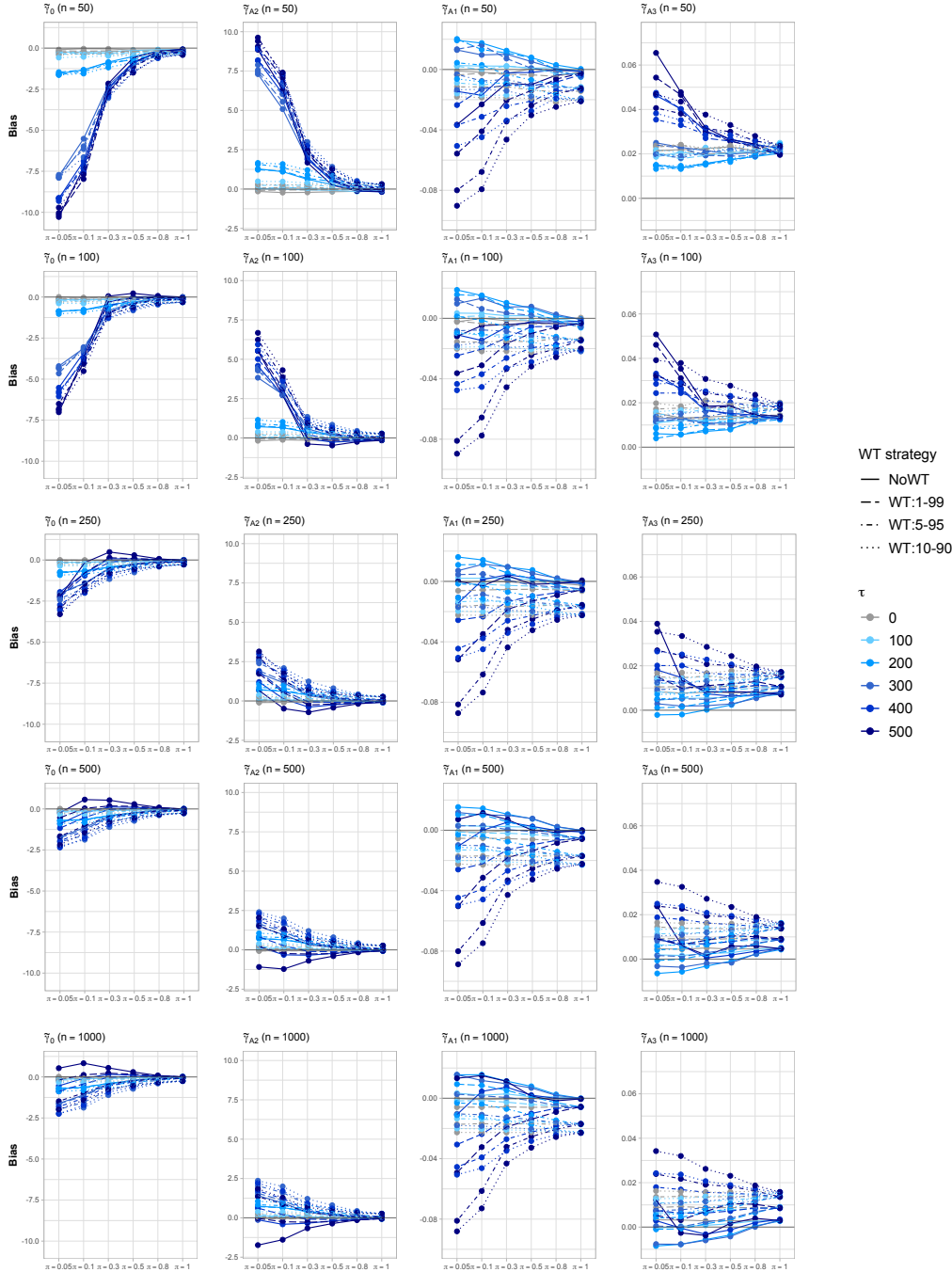


**Figure S1:** Bias of the coefficient estimates for the different setting of simulation study I. Each column refer to a different coefficient ( $\tilde{\gamma}_0$ : first column;  $\tilde{\gamma}_{A1}$ : third column;  $\tilde{\gamma}_{A2}$ : second column;  $\tilde{\gamma}_{A3}$ : fourth column). Each row refers to a different sample size  $n = 50, 100, 250, 500, 1000$ . The x-axes show the compliance-threshold values  $\pi$ . Different types of line refer to different weight truncation (WT) strategies (solid: No WT; long-dashed: 1-99 WT; dot-dashed: 5-95 WT; dotted: 10-90 WT). The colours refer to different values of the rule-threshold  $\tau$ : the darker the colour, the more severe the violation (i.e., the higher  $\tau$ ). Note that the ranges of y-axes differ between panels.

## EmpSE for estimated regression coefficients of logit-MSM (9)

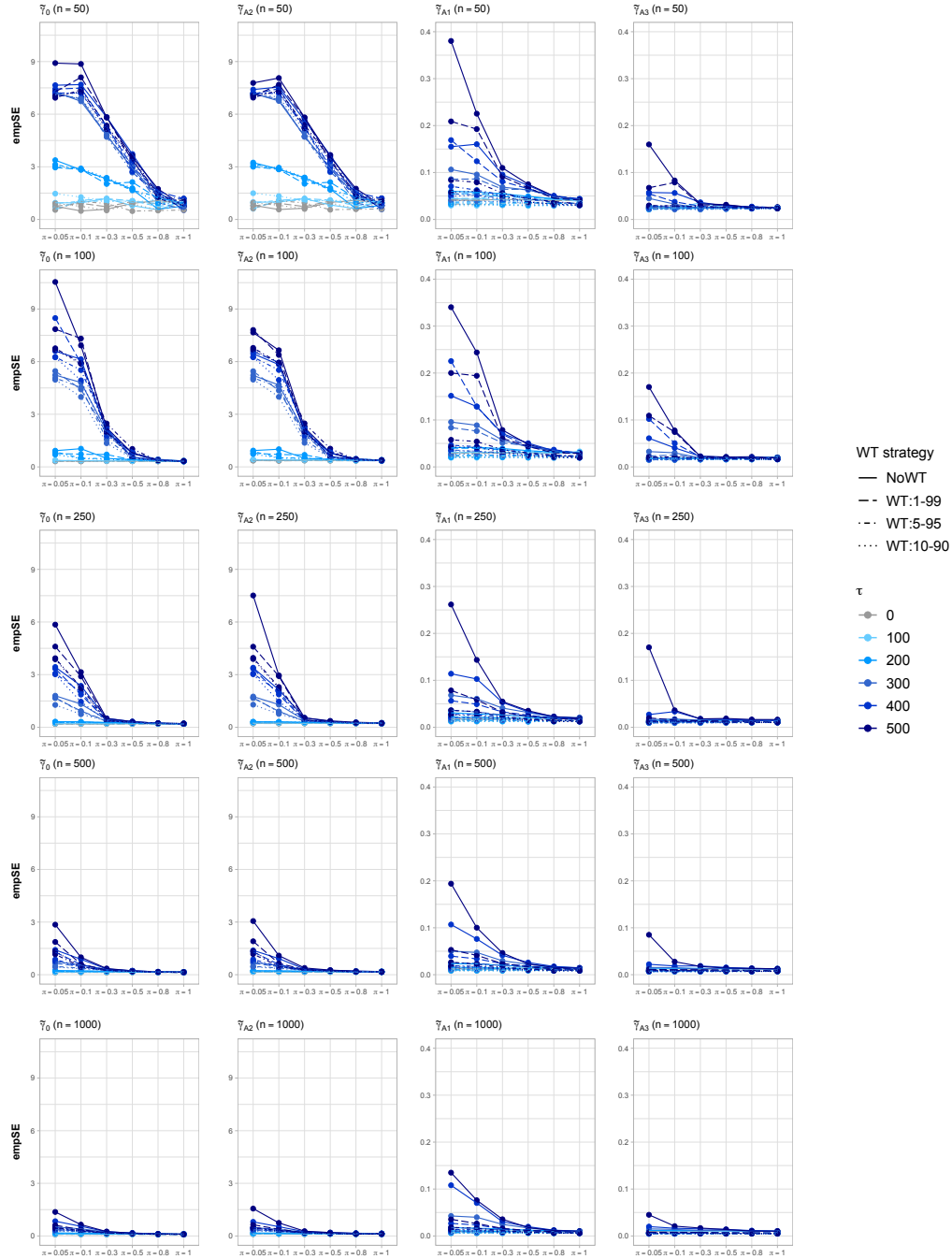


**Figure S2:** Empirical Standard Error (empSE) of the coefficient estimates for the different setting of simulation study I. Each column refer to a different coefficient ( $\tilde{\gamma}_0$ : first column;  $\tilde{\gamma}_{A1}$ : third column;  $\tilde{\gamma}_{A2}$ : second column;  $\tilde{\gamma}_{A3}$ : fourth column). Each row refers to a different sample size  $n = 50, 100, 250, 500, 1000$ . The x-axes show the compliance-threshold values  $\pi$ . Different types of line refer to different weight truncation (WT) strategies (solid: No WT; long-dashed: 1-99 WT; dot-dashed: 5-95 WT; dotted: 10-90 WT). The colours refer to different values of the rule-threshold  $\tau$ : the darker the colour, the more severe the violation (i.e., the higher  $\tau$ ). Note that the ranges of y-axes differ between panels.

### RMSE for estimated regression coefficients of logit-MSM (9)

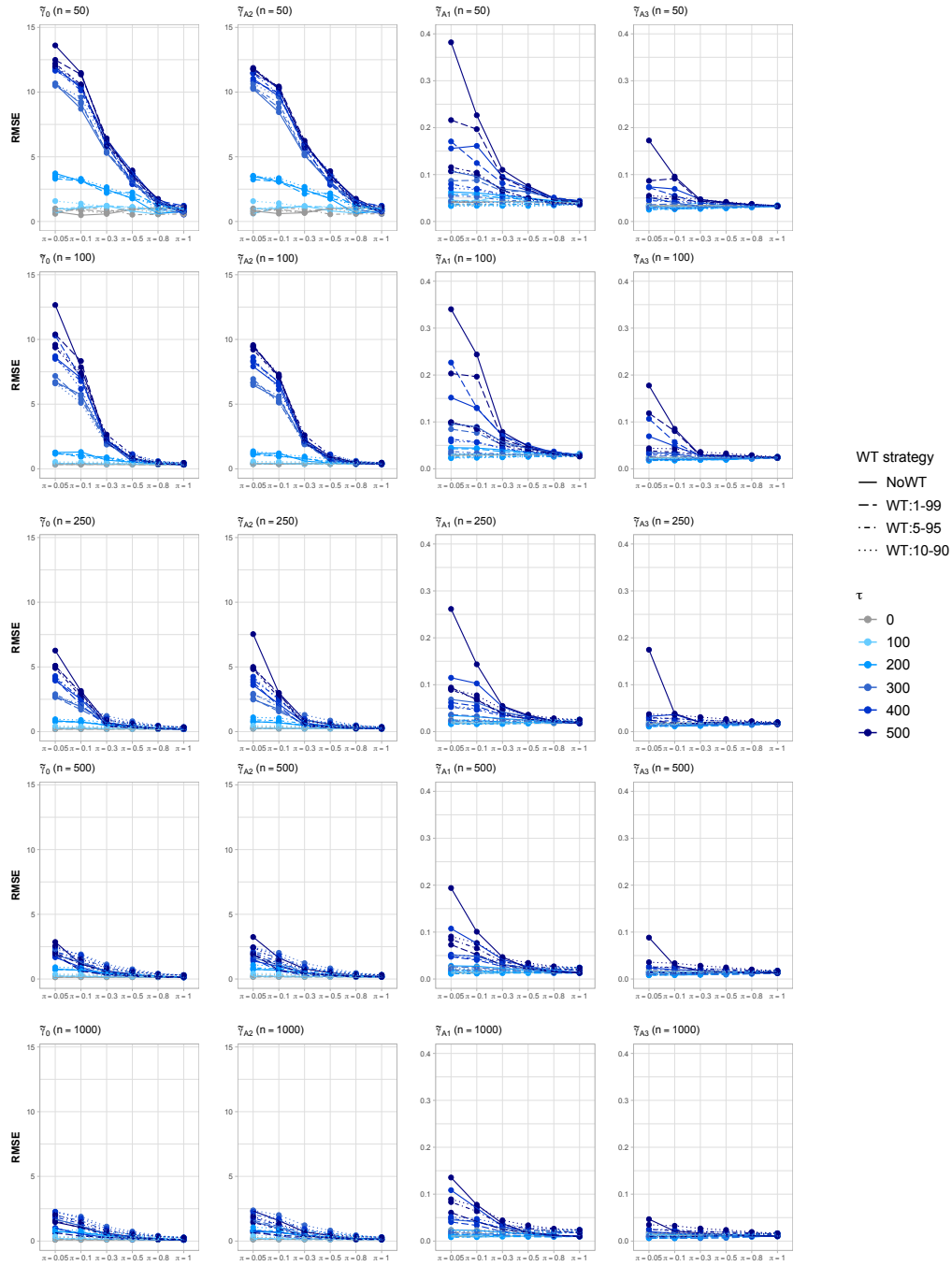


**Figure S3:** Root Mean Squared Error (RMSE) of the coefficient estimates for the different setting of simulation study I. Each column refer to a different coefficient ( $\tilde{\gamma}_0$ : first column;  $\tilde{\gamma}_{A1}$ : third column;  $\tilde{\gamma}_{A2}$ : second column;  $\tilde{\gamma}_{A3}$ : fourth column). Each row refers to a different sample size  $n = 50, 100, 250, 500, 1000$ . The x-axes show the compliance-threshold values  $\pi$ . Different types of line refer to different weight truncation (WT) strategies (solid: No WT; long-dashed: 1-99 WT; dot-dashed: 5-95 WT; dotted: 10-90 WT). The colours refer to different values of the rule-threshold  $\tau$ : the darker the colour, the more severe the violation (i.e., the higher  $\tau$ ). Note that the ranges of y-axes differ between panels.

## S2 Simulation study II: additional results

### S2.1 Bias

Bias for  $\hat{C}_0(t)$  estimated from Aalen-MSM (12)

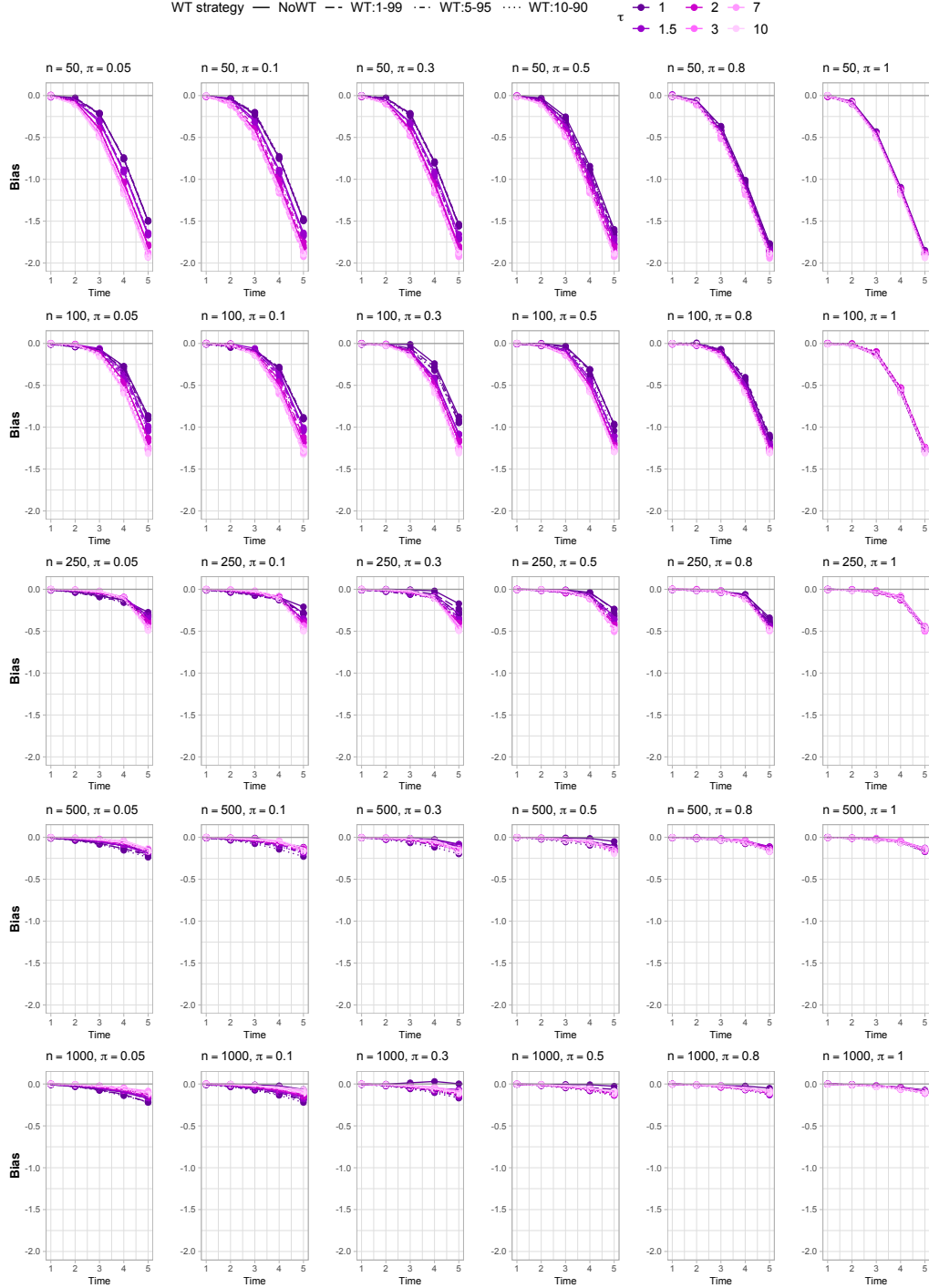


**Figure S4:** Bias of the estimates for the cumulative coefficient  $C_0(t) = \int_0^t \tilde{\alpha}_0(s)ds$  at time points  $t = 1, \dots, 5$  for the different setting of simulation study II. Each row refers to a different sample size  $n = 50, 100, 250, 500, 1000$ . Each column refers to a different exposure cut-off  $\pi = 0.05, 0.1, 0.3, 0.5, 0.8, 1$ . Different types of line refer to different weight truncation (WT) strategies (solid: No WT; long-dashed: 1-99 WT; dot-dashed: 5-95 WT; dotted: 10-90 WT). The colours refer to different values of the rule-threshold  $\tau$ : the darker the colour, the more severe the violation (i.e., the lower  $\tau$ ).

## Bias for $\hat{C}_{A_0}(t)$ estimated from Aalen-MSM (12)

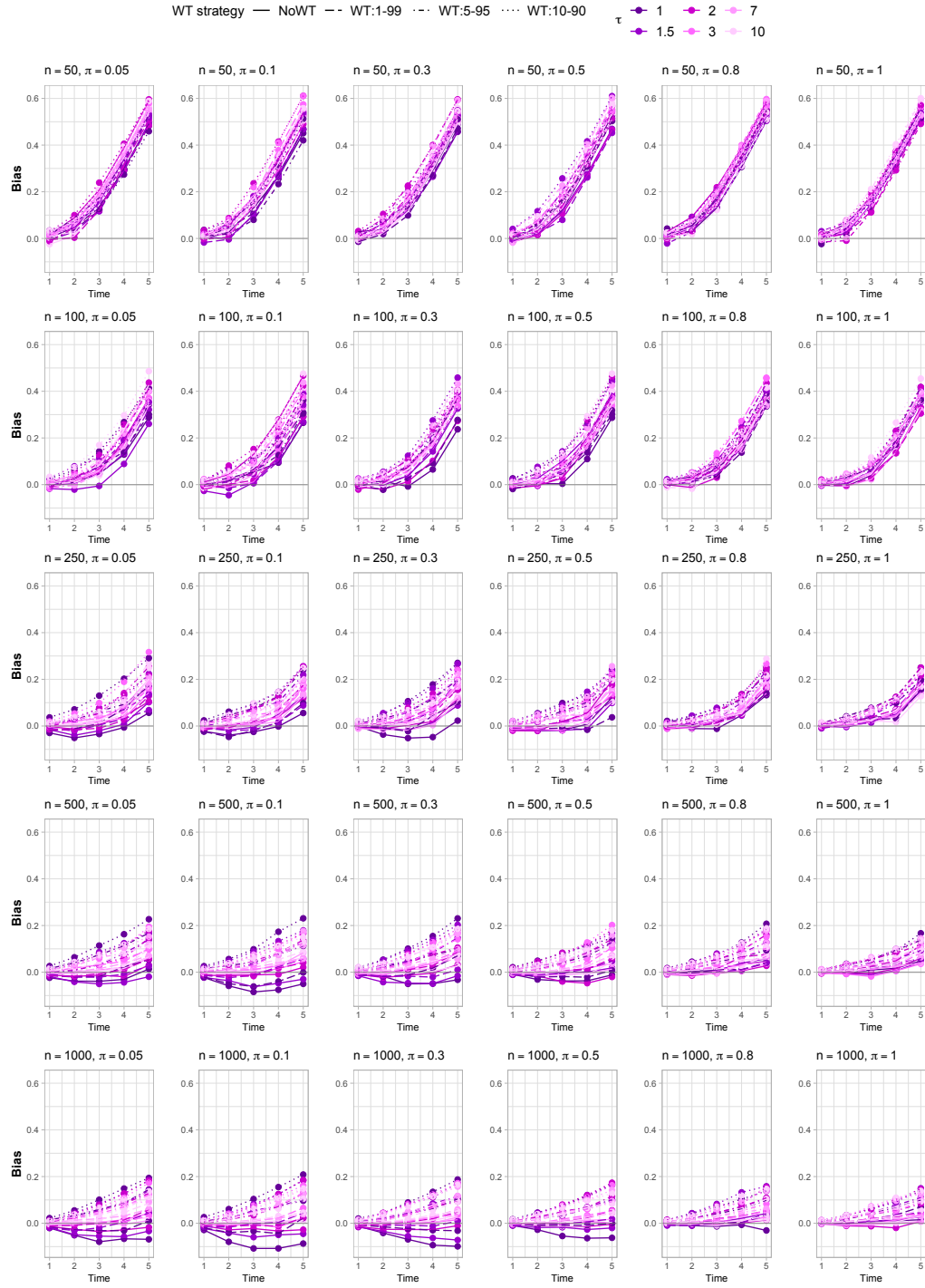


**Figure S5:** Bias of the estimates for the cumulative coefficient  $C_{A_0}(t) = \int_0^t \tilde{\alpha}_{A_0}(s) ds$  at time points  $t = 1, \dots, 5$  for the different setting of simulation study II. Each row refers to a different sample size  $n = 50, 100, 250, 500, 1000$ . Each column refers to a different exposure cut-off  $\pi = 0.05, 0.1, 0.3, 0.5, 0.8, 1$ . Different types of line refer to different weight truncation (WT) strategies (solid: No WT; long-dashed: 1-99 WT; dot-dashed: 5-95 WT; dotted: 10-90 WT). The colours refer to different values of the rule-threshold  $\tau$ : the darker the colour, the more severe the violation (i.e., the lower  $\tau$ ).



## Bias for $\hat{C}_{A_1}(t)$ estimated from Aalen-MSM (12)

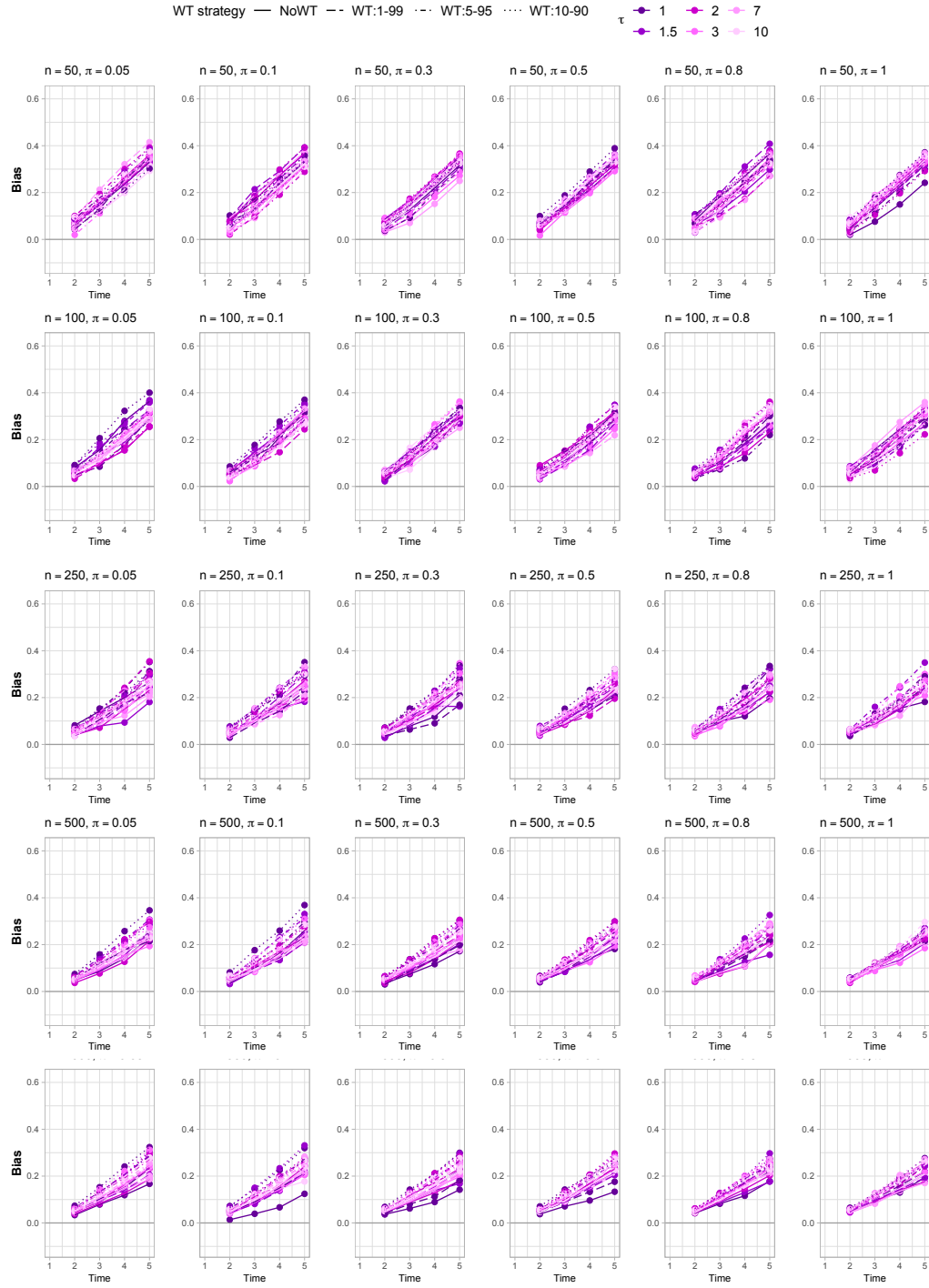


**Figure S6:** Bias of the estimates for the cumulative coefficient  $C_{A_1}(t) = \int_1^t \tilde{\alpha}_{A_1}(s)ds$  at time points  $t = 2, 3, 4, 5$  for the different setting of simulation study II. Each row refers to a different sample size  $n = 50, 100, 250, 500, 1000$ . Each column refers to a different exposure cut-off  $\pi = 0.05, 0.1, 0.3, 0.5, 0.8, 1$ . Different types of line refer to different weight truncation (WT) strategies (solid: No WT; long-dashed: 1-99 WT; dot-dashed: 5-95 WT; dotted: 10-90 WT). The colours refer to different values of the rule-threshold  $\tau$ : the darker the colour, the more severe the violation (i.e., the lower  $\tau$ ).

## Bias for $\hat{C}_{A_2}(t)$ estimated from Aalen-MSM (12)

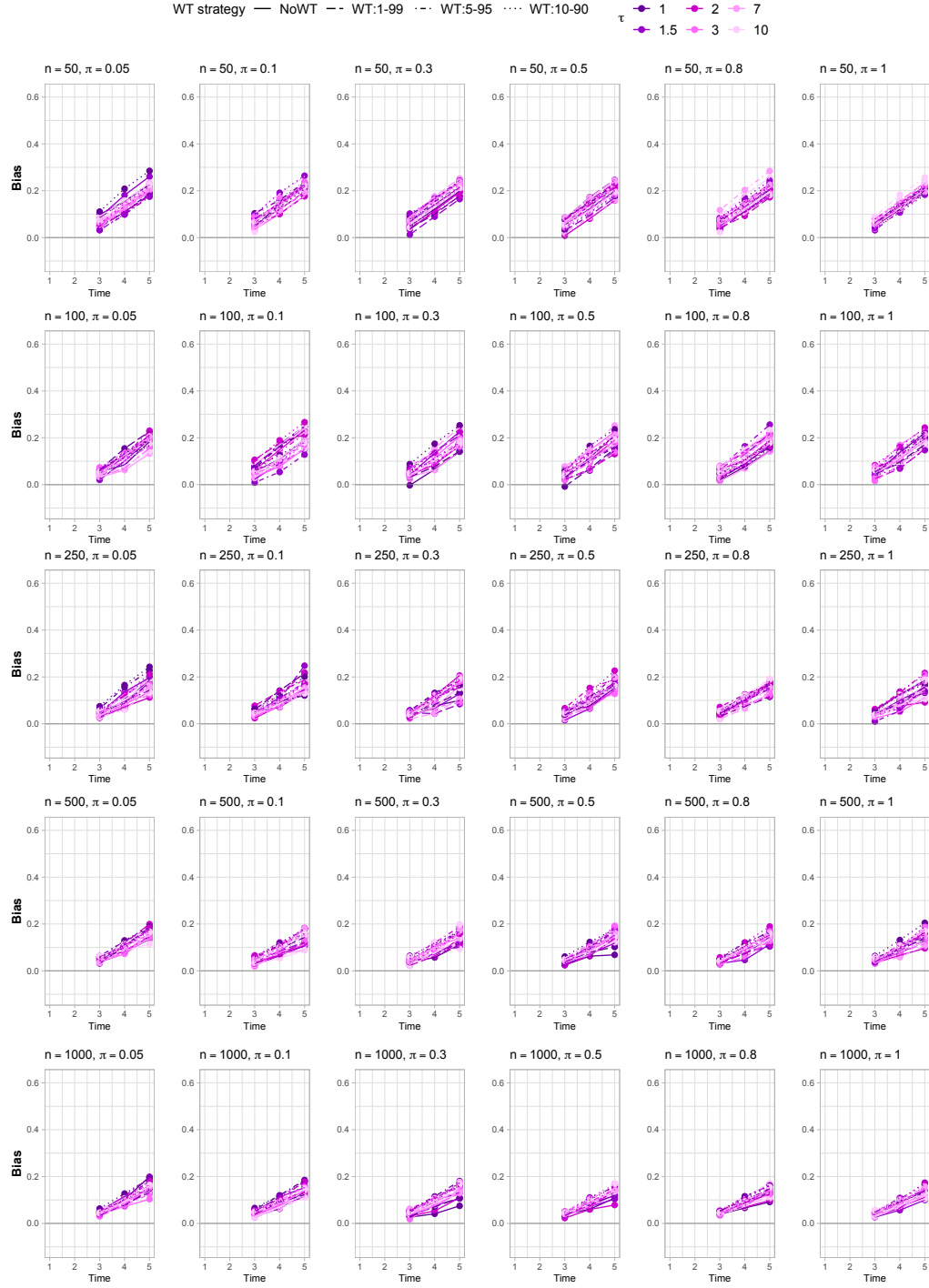


**Figure S7:** Bias of the estimates for the cumulative coefficient  $C_{A_2}(t) = \int_2^t \tilde{\alpha}_{A_2}(s)ds$  at time points  $t = 3, 4, 5$  for the different setting of simulation study II. Each row refers to a different sample size  $n = 50, 100, 250, 500, 1000$ . Each column refers to a different exposure cut-off  $\pi = 0.05, 0.1, 0.3, 0.5, 0.8, 1$ . Different types of line refer to different weight truncation (WT) strategies (solid: No WT; long-dashed: 1-99 WT; dot-dashed: 5-95 WT; dotted: 10-90 WT). The colours refer to different values of the rule-threshold  $\tau$ : the darker the colour, the more severe the violation (i.e., the lower  $\tau$ ).

## Bias for $\hat{C}_{A_3}(t)$ estimated from Aalen-MSM (12)

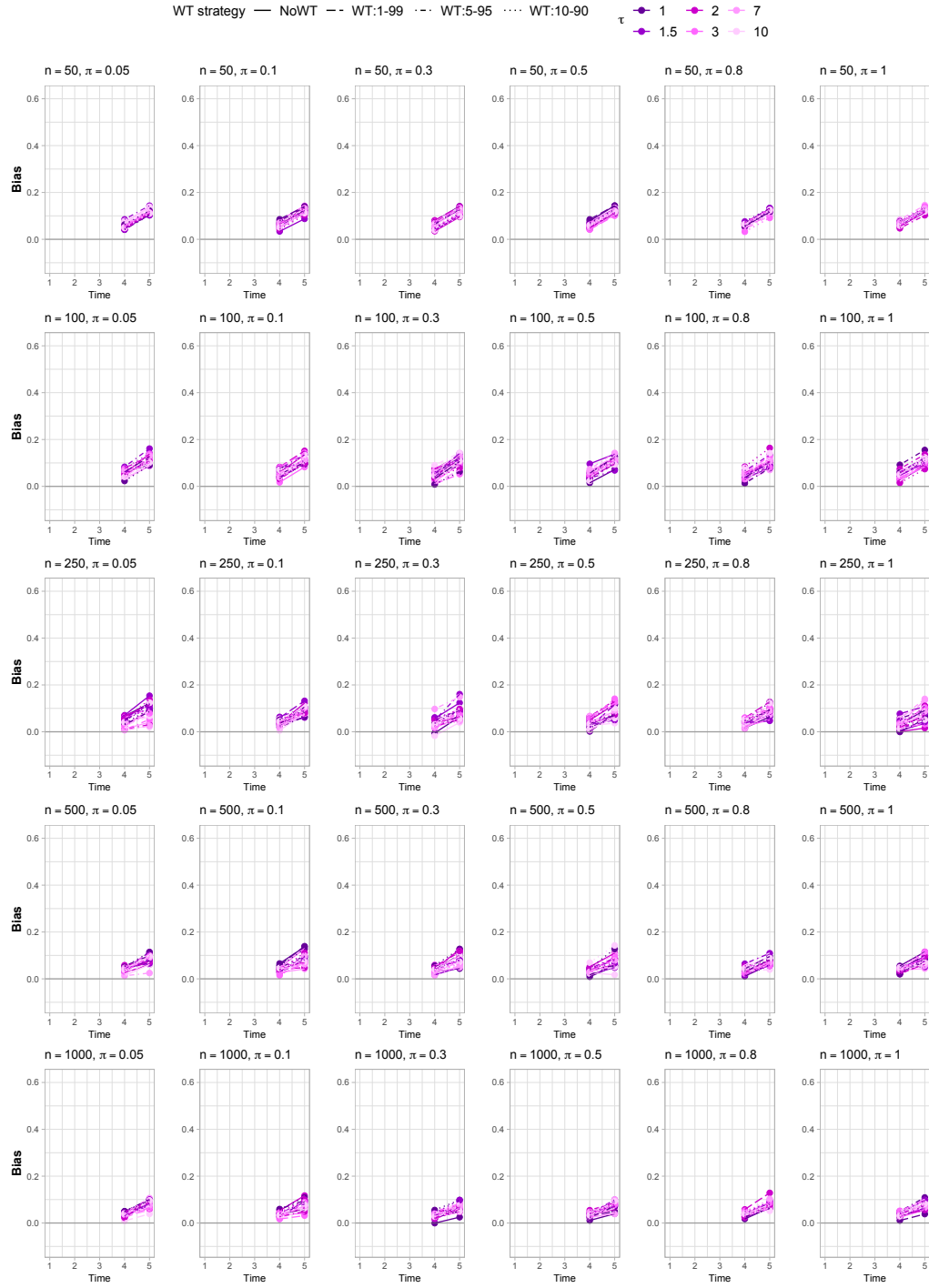


**Figure S8:** Bias of the estimates for the cumulative coefficient  $C_{A_3}(t) = \int_3^t \tilde{\alpha}_{A_3}(s)ds$  at time points  $t = 4, 5$  for the different setting of simulation study II. Each row refers to a different sample size  $n = 50, 100, 250, 500, 1000$ . Each column refers to a different exposure cut-off  $\pi = 0.05, 0.1, 0.3, 0.5, 0.8, 1$ . Different types of line refer to different weight truncation (WT) strategies (solid: No WT; long-dashed: 1-99 WT; dot-dashed: 5-95 WT; dotted: 10-90 WT). The colours refer to different values of the rule-threshold  $\tau$ : the darker the colour, the more severe the violation (i.e., the lower  $\tau$ ).

### Bias for $\hat{C}_{A_4}(t = 5)$ estimated from Aalen-MSM (12)

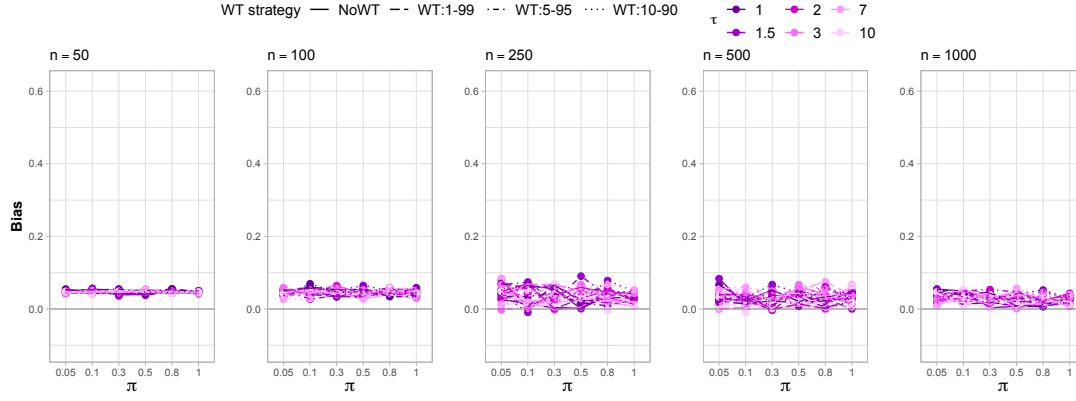


**Figure S9:** Bias of the estimates for the cumulative coefficient  $C_{A4}(t = 5) = \int_4^5 \tilde{\alpha}_{A4}(s)ds$  for the different setting of simulation study II. Each column refers to a different sample size  $n = 50, 100, 250, 500, 1000$ . The x-axes show the compliance-threshold values  $\pi = 0.05, 0.1, 0.3, 0.5, 0.8, 1$ . Different types of line refer to different weight truncation (WT) strategies (solid: No WT; long-dashed: 1-99 WT; dot-dashed: 5-95 WT; dotted: 10-90 WT). The colours refer to different values of the rule-threshold  $\tau$ : the darker the colour, the more severe the violation (i.e., the lower  $\tau$ ).

## S2.2 Empirical standard error

EmpSE for  $\hat{C}_0(t)$  estimated from Aalen-MSM (12)

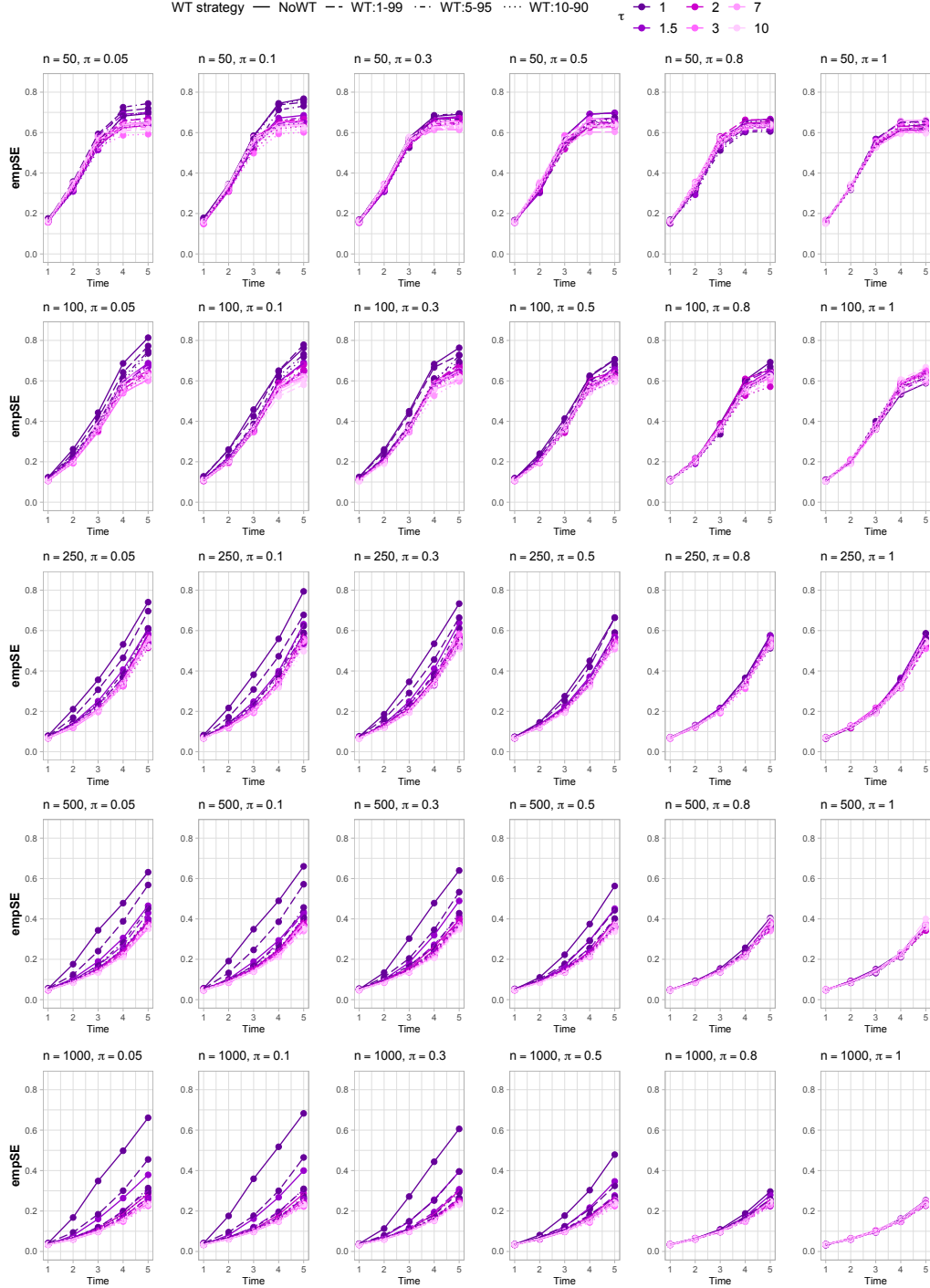


**Figure S10:** Empirical Standard Error (empSE) of the estimates for the cumulative coefficient  $C_0(t) = \int_0^t \tilde{\alpha}_0(s)ds$  at time points  $t = 1, \dots, 5$  for the different setting of simulation study II. Each row refers to a different sample size  $n = 50, 100, 250, 500, 1000$ . Each column refers to a different exposure cut-off  $\pi = 0.05, 0.1, 0.3, 0.5, 0.8, 1$ . Different types of line refer to different weight truncation (WT) strategies (solid: No WT; long-dashed: 1-99 WT; dot-dashed: 5-95 WT; dotted: 10-90 WT). The colours refer to different values of the rule-threshold  $\tau$ : the darker the colour, the more severe the violation (i.e., the lower  $\tau$ ).

## EmpSE for $\hat{C}_{A_0}(t)$ estimated from Aalen-MSM (12)

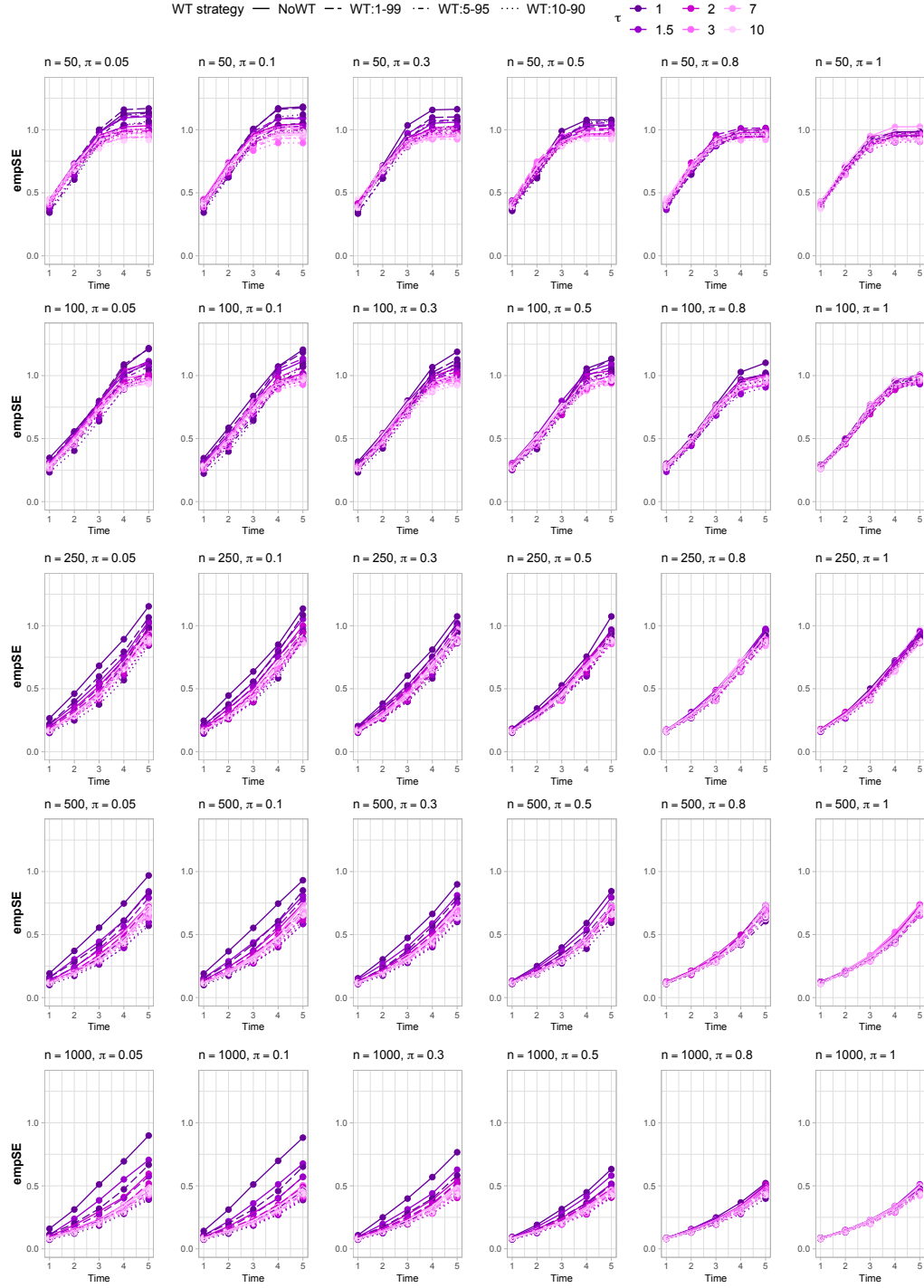


**Figure S11:** Empirical Standard Error (empSE) of the estimates for the cumulative coefficient  $C_{A_0}(t) = \int_0^t \tilde{\alpha}_{A_0}(s)ds$  at time points  $t = 1, \dots, 5$  for the different setting of simulation study II. Each row refers to a different sample size  $n = 50, 100, 250, 500, 1000$ . Each column refers to a different exposure cut-off  $\pi = 0.05, 0.1, 0.3, 0.5, 0.8, 1$ . Different types of line refer to different weight truncation (WT) strategies (solid: No WT; long-dashed: 1-99 WT; dot-dashed: 5-95 WT; dotted: 10-90 WT). The colours refer to different values of the rule-threshold  $\tau$ : the darker the colour, the more severe the violation (i.e., the lower  $\tau$ ).

## EmpSE for $\hat{C}_{A1}(t)$ estimated from Aalen-MSM (12)

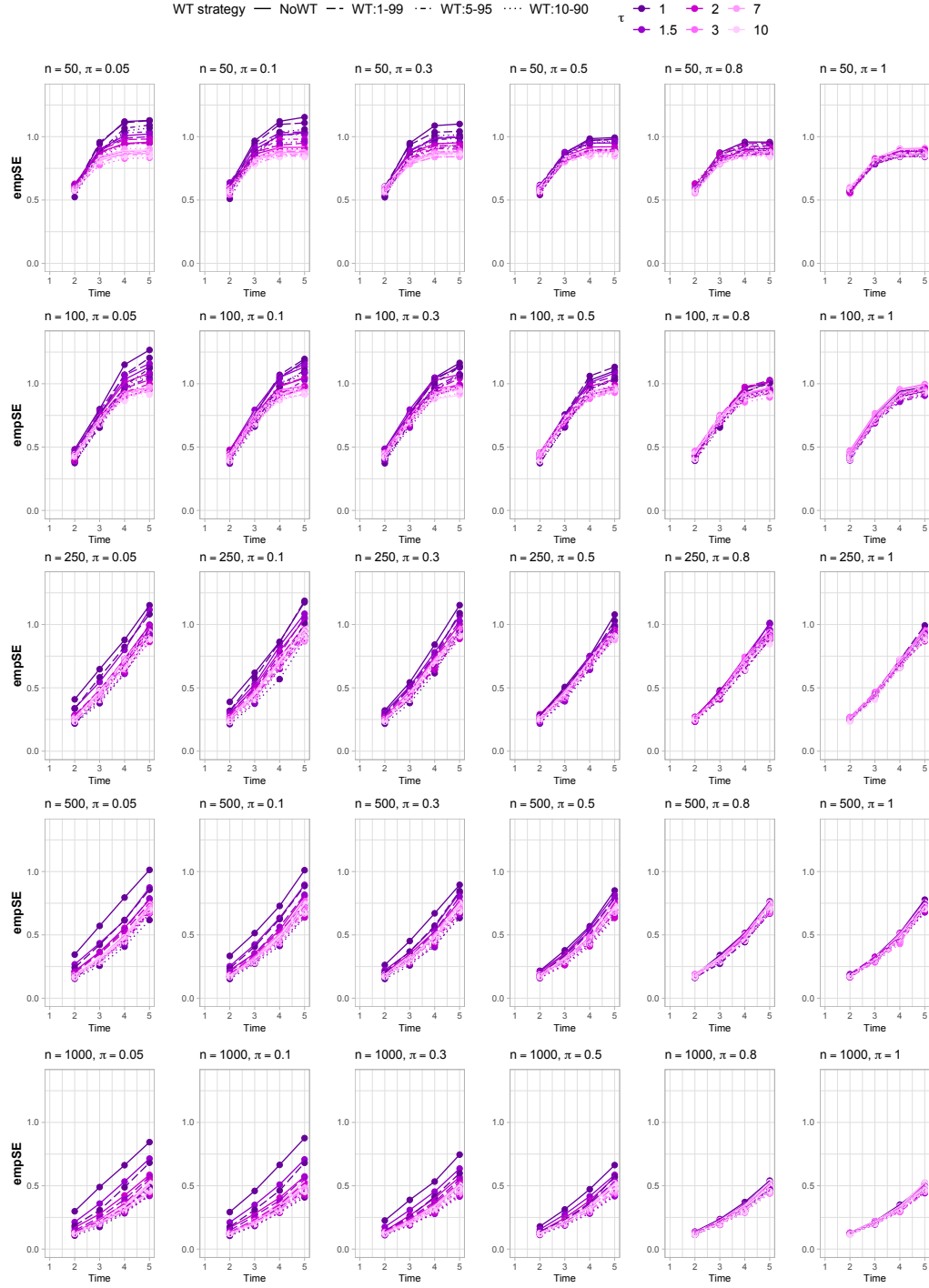


**Figure S12:** Empirical Standard Error (empSE) of the estimates for the cumulative coefficient  $C_{A1}(t) = \int_1^t \tilde{\alpha}_{A1}(s)ds$  at time points  $t = 2, 3, 4, 5$  for the different setting of simulation study II. Each row refers to a different sample size  $n = 50, 100, 250, 500, 1000$ . Each column refers to a different exposure cut-off  $\pi = 0.05, 0.1, 0.3, 0.5, 0.8, 1$ . Different types of line refer to different weight truncation (WT) strategies (solid: No WT; long-dashed: 1-99 WT; dot-dashed: 5-95 WT; dotted: 10-90 WT). The colours refer to different values of the rule-threshold  $\tau$ : the darker the colour, the more severe the violation (i.e., the lower  $\tau$ ).



### EmpSE for $\hat{C}_{A_2}(t)$ estimated from Aalen-MSM (12)

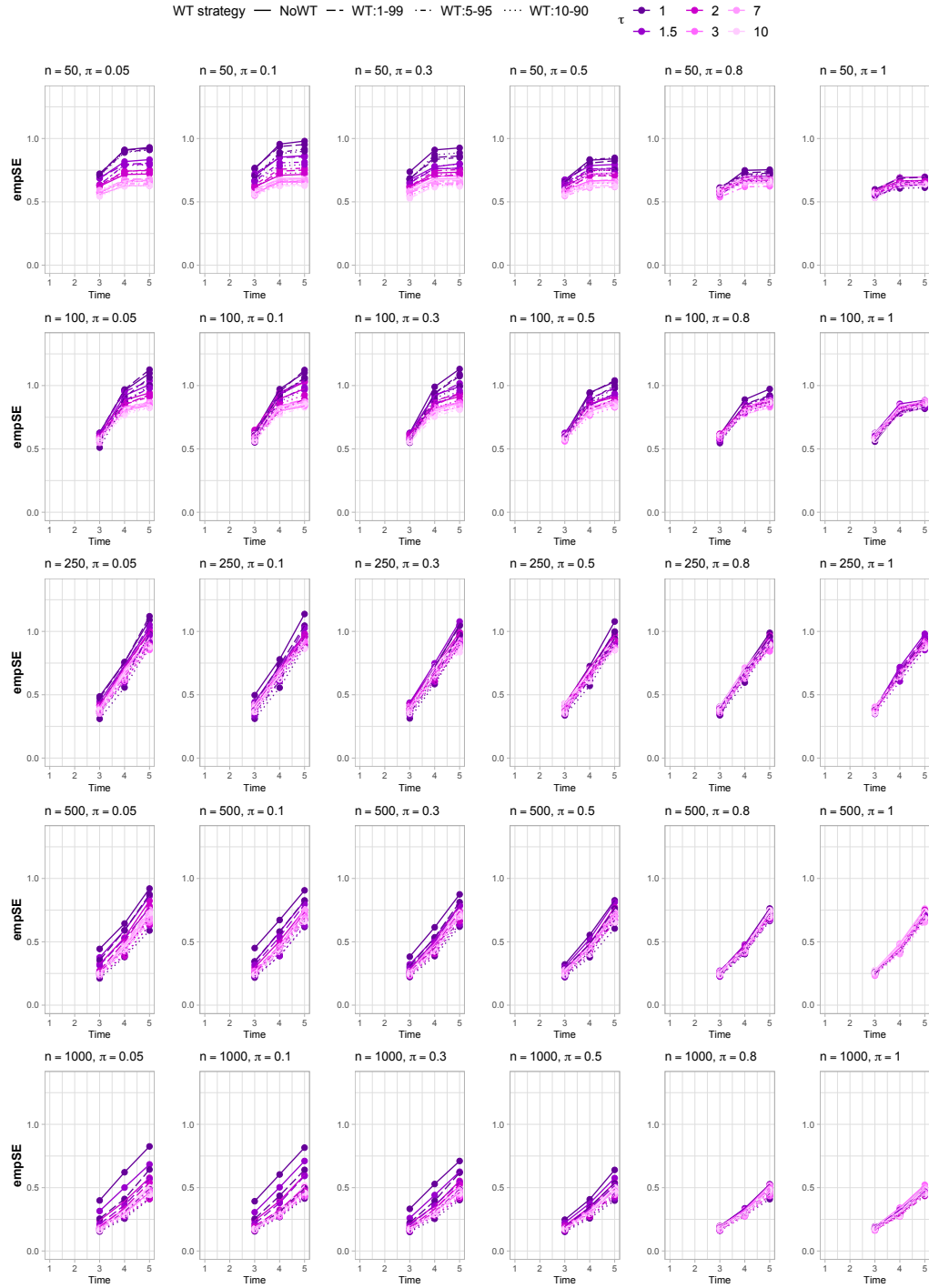


**Figure S13:** Empirical Standard Error (empSE) of the estimates for the cumulative coefficient  $C_{A_2}(t) = \int_2^t \tilde{\alpha}_{A_2}(s)ds$  at time points  $t = 3, 4, 5$  for the different setting of simulation study II. Each row refers to a different sample size  $n = 50, 100, 250, 500, 1000$ . Each column refers to a different exposure cut-off  $\pi = 0.05, 0.1, 0.3, 0.5, 0.8, 1$ . Different types of line refer to different weight truncation (WT) strategies (solid: No WT; long-dashed: 1-99 WT; dot-dashed: 5-95 WT; dotted: 10-90 WT). The colours refer to different values of the rule-threshold  $\tau$ : the darker the colour, the more severe the violation (i.e., the lower  $\tau$ ).

## EmpSE for $\hat{C}_{A_3}(t)$ estimated from Aalen-MSM (12)

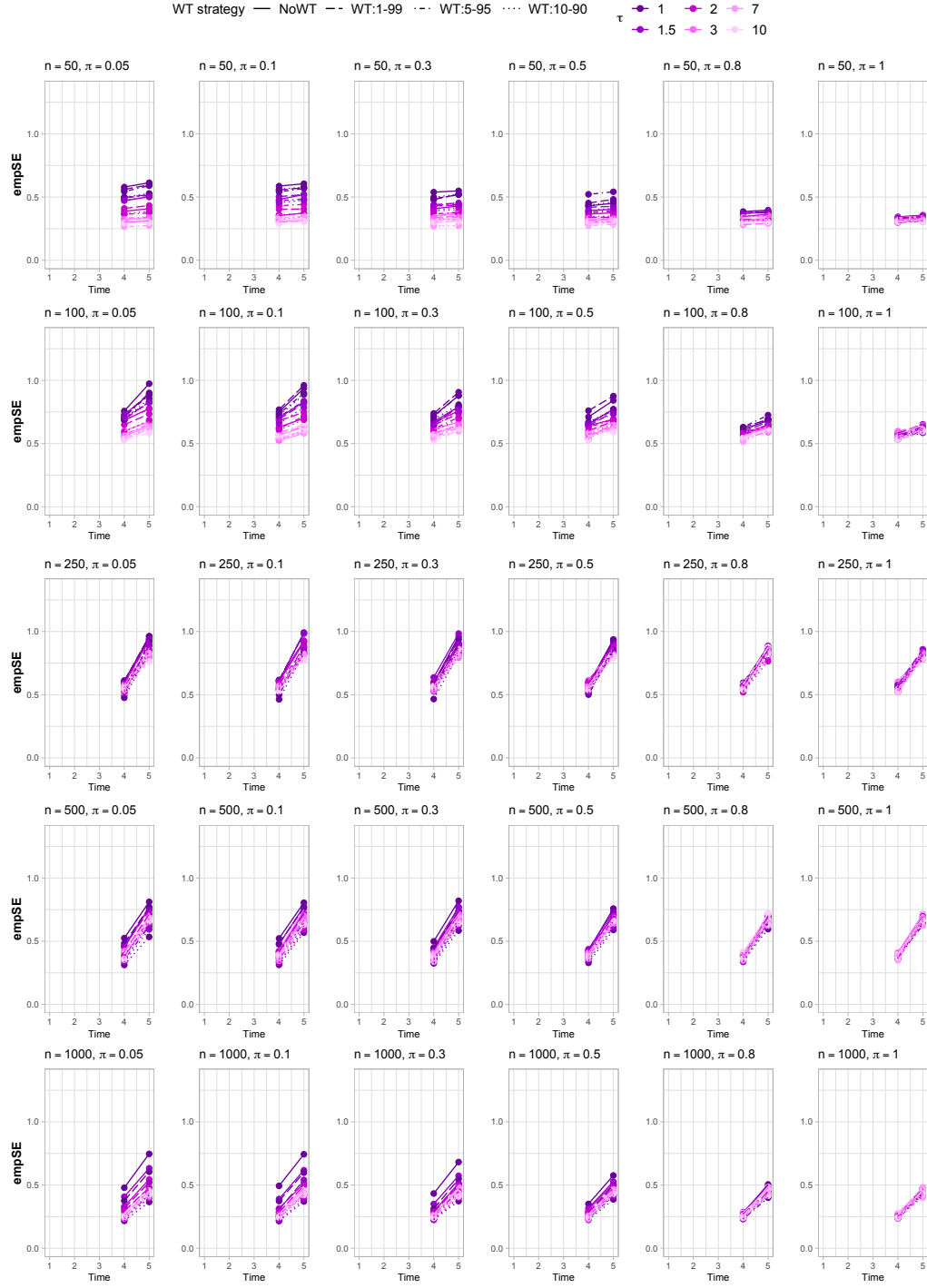


**Figure S14:** Empirical Standard Error (empSE) of the estimates for the cumulative coefficient  $C_{A_3}(t) = \int_3^t \tilde{\alpha}_{A_3}(s) ds$  at time points  $t = 4, 5$  for the different setting of simulation study II. Each row refers to a different sample size  $n = 50, 100, 250, 500, 1000$ . Each column refers to a different exposure cut-off  $\pi = 0.05, 0.1, 0.3, 0.5, 0.8, 1$ . Different types of line refer to different weight truncation (WT) strategies (solid: No WT; long-dashed: 1-99 WT; dot-dashed: 5-95 WT; dotted: 10-90 WT). The colours refer to different values of the rule-threshold  $\tau$ : the darker the colour, the more severe the violation (i.e., the lower  $\tau$ ).

# EmpSE for $\hat{C}_{A_4}(t = 5)$ estimated from Aalen-MSM (12)

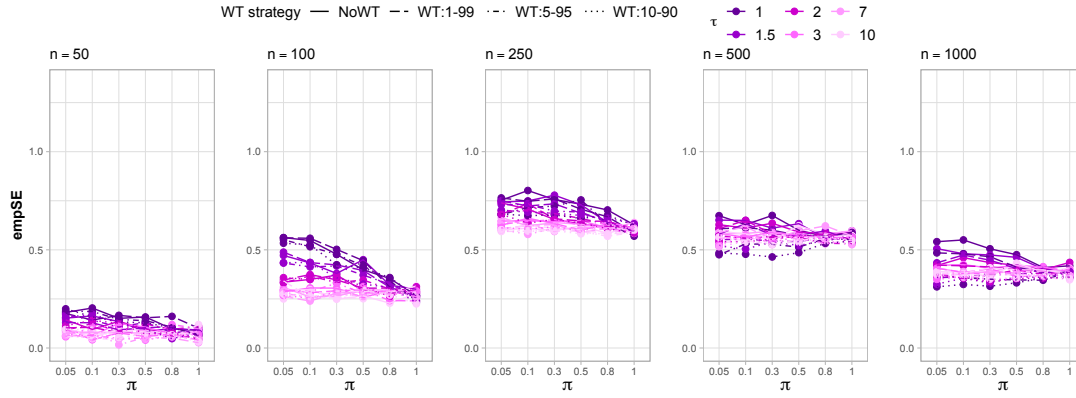


**Figure S15:** Empirical Standard Error (empSE) of the estimates for the cumulative coefficient  $C_{A4}(t = 5) = \int_4^5 \tilde{\alpha}_{A4}(s)ds$  for the different setting of simulation study II. Each column refers to a different sample size  $n = 50, 100, 250, 500, 1000$ . The x-axes show the compliance-threshold values  $\pi = 0.05, 0.1, 0.3, 0.5, 0.8, 1$ . Different types of line refer to different weight truncation (WT) strategies (solid: No WT; long-dashed: 1-99 WT; dot-dashed: 5-95 WT; dotted: 10-90 WT). The colours refer to different values of the rule-threshold  $\tau$ : the darker the colour, the more severe the violation (i.e., the lower  $\tau$ ).

## S2.3 Root mean squared error

RMSE for  $\hat{C}_0(t)$  estimated from Aalen-MSM (12)

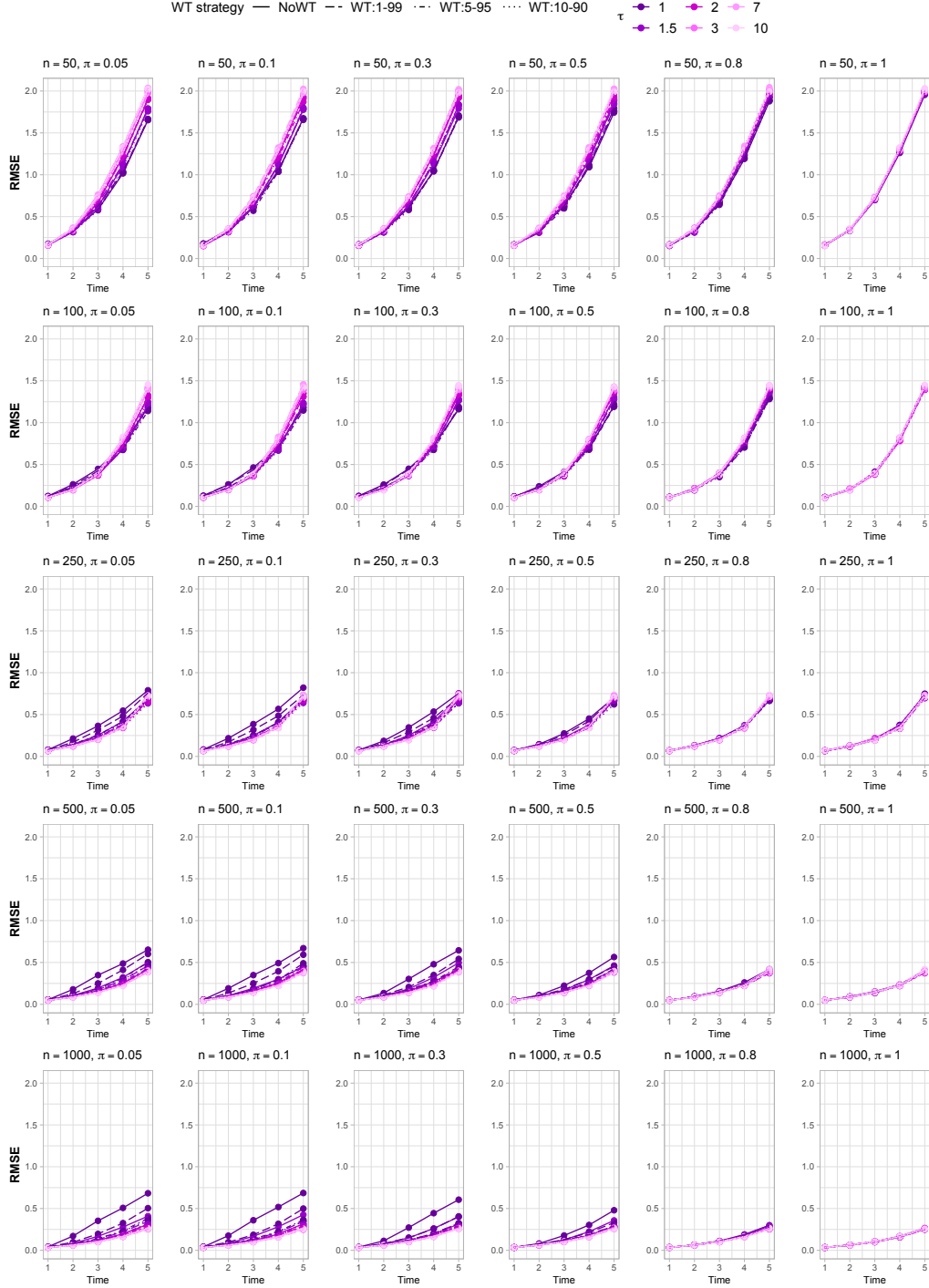


**Figure S16:** Root Mean Squared Error (RMSE) of the estimates for the cumulative coefficient  $C_0(t) = \int_0^t \tilde{\alpha}_0(s)ds$  at time points  $t = 1, \dots, 5$  for the different setting of simulation study II. Each row refers to a different sample size  $n = 50, 100, 250, 500, 1000$ . Each column refers to a different exposure cut-off  $\pi = 0.05, 0.1, 0.3, 0.5, 0.8, 1$ . Different types of line refer to different weight truncation (WT) strategies (solid: No WT; long-dashed: 1-99 WT; dot-dashed: 5-95 WT; dotted: 10-90 WT). The colours refer to different values of the rule-threshold  $\tau$ : the darker the colour, the more severe the violation (i.e., the lower  $\tau$ ).

## RMSE for $\hat{C}_{A_0}(t)$ estimated from Aalen-MSM (12)

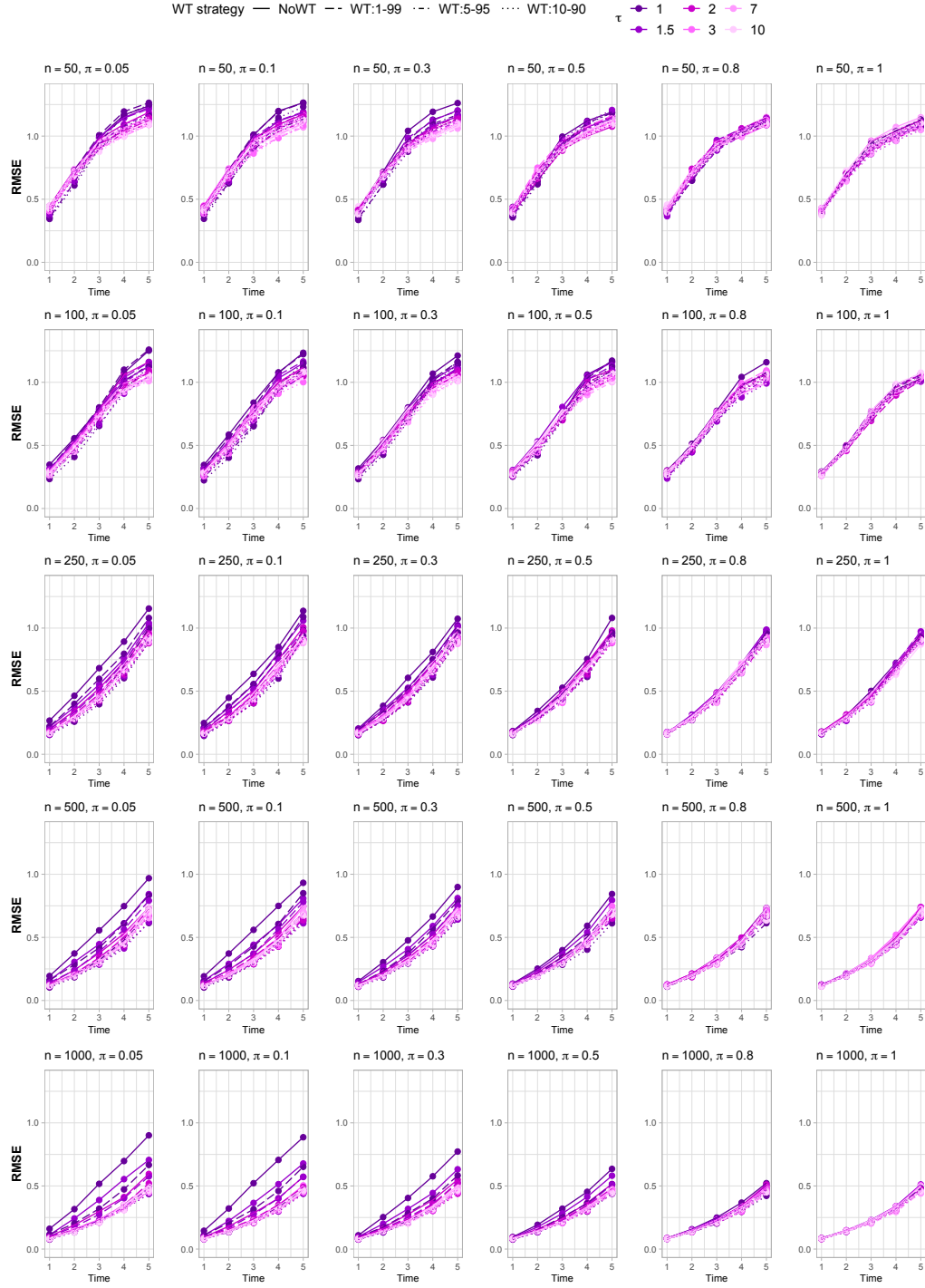


**Figure S17:** Root Mean Squared Error (RMSE) of the estimates for the cumulative coefficient  $C_{A_0}(t) = \int_0^t \tilde{\alpha}_{A_0}(s)ds$  at time points  $t = 1, \dots, 5$  for the different setting of simulation study II. Each row refers to a different sample size  $n = 50, 100, 250, 500, 1000$ . Each column refers to a different exposure cut-off  $\pi = 0.05, 0.1, 0.3, 0.5, 0.8, 1$ . Different types of line refer to different weight truncation (WT) strategies (solid: No WT; long-dashed: 1-99 WT; dot-dashed: 5-95 WT; dotted: 10-90 WT). The colours refer to different values of the rule-threshold  $\tau$ : the darker the colour, the more severe the violation (i.e., the lower  $\tau$ ).

## RMSE for $\hat{C}_{A_1}(t)$ estimated from Aalen-MSM (12)

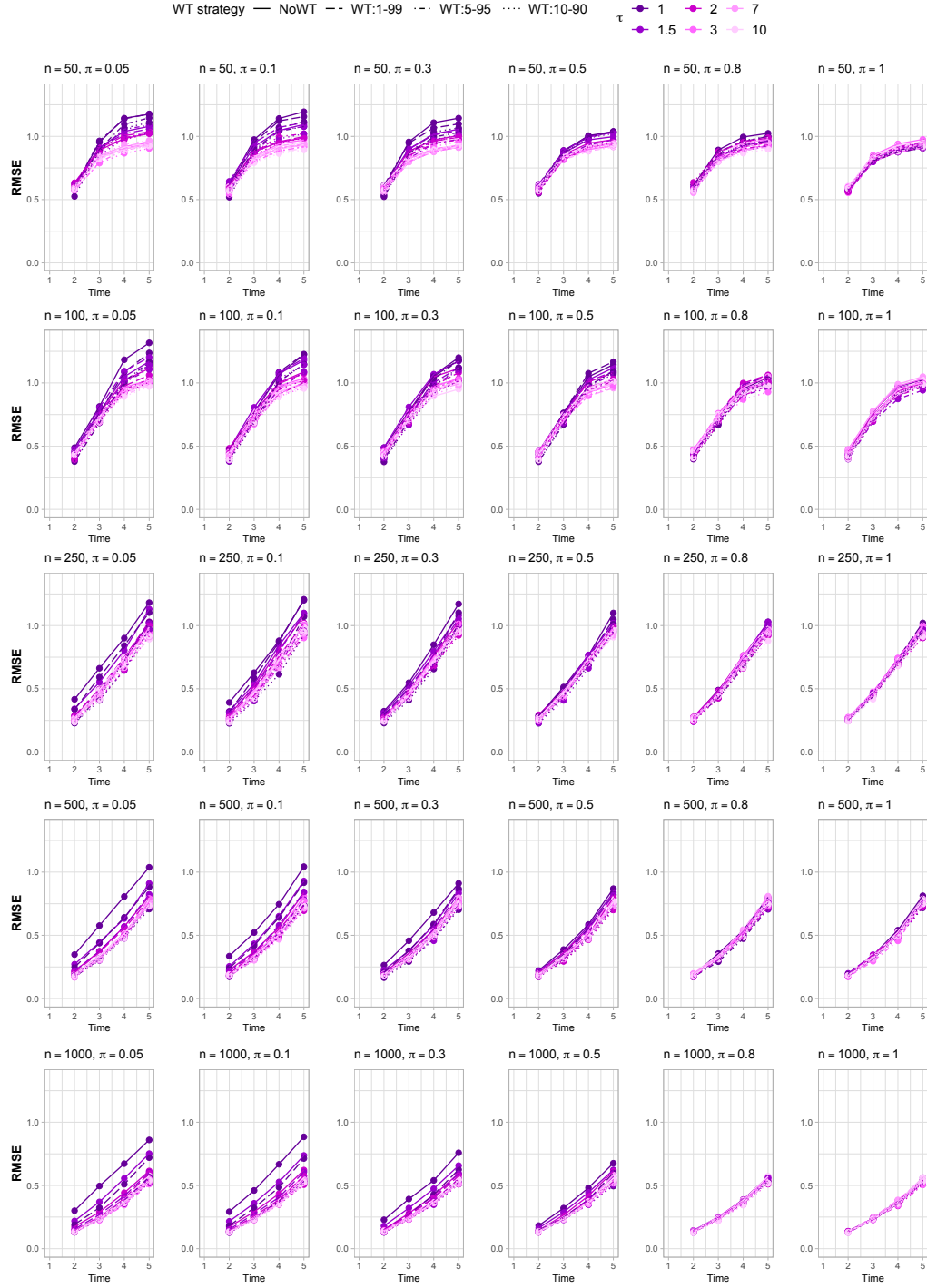


**Figure S18:** Root Mean Squared Error (RMSE) of the estimates for the cumulative coefficient  $C_{A_1}(t) = \int_1^t \tilde{\alpha}_{A_1}(s)ds$  at time points  $t = 2, 3, 4, 5$  for the different setting of simulation study II. Each row refers to a different sample size  $n = 50, 100, 250, 500, 1000$ . Each column refers to a different exposure cut-off  $\pi = 0.05, 0.1, 0.3, 0.5, 0.8, 1$ . Different types of line refer to different weight truncation (WT) strategies (solid: No WT; long-dashed: 1-99 WT; dot-dashed: 5-95 WT; dotted: 10-90 WT). The colours refer to different values of the rule-threshold  $\tau$ : the darker the colour, the more severe the violation (i.e., the lower  $\tau$ ).

# RMSE for $\hat{C}_{A_2}(t)$ estimated from Aalen-MSM (12)

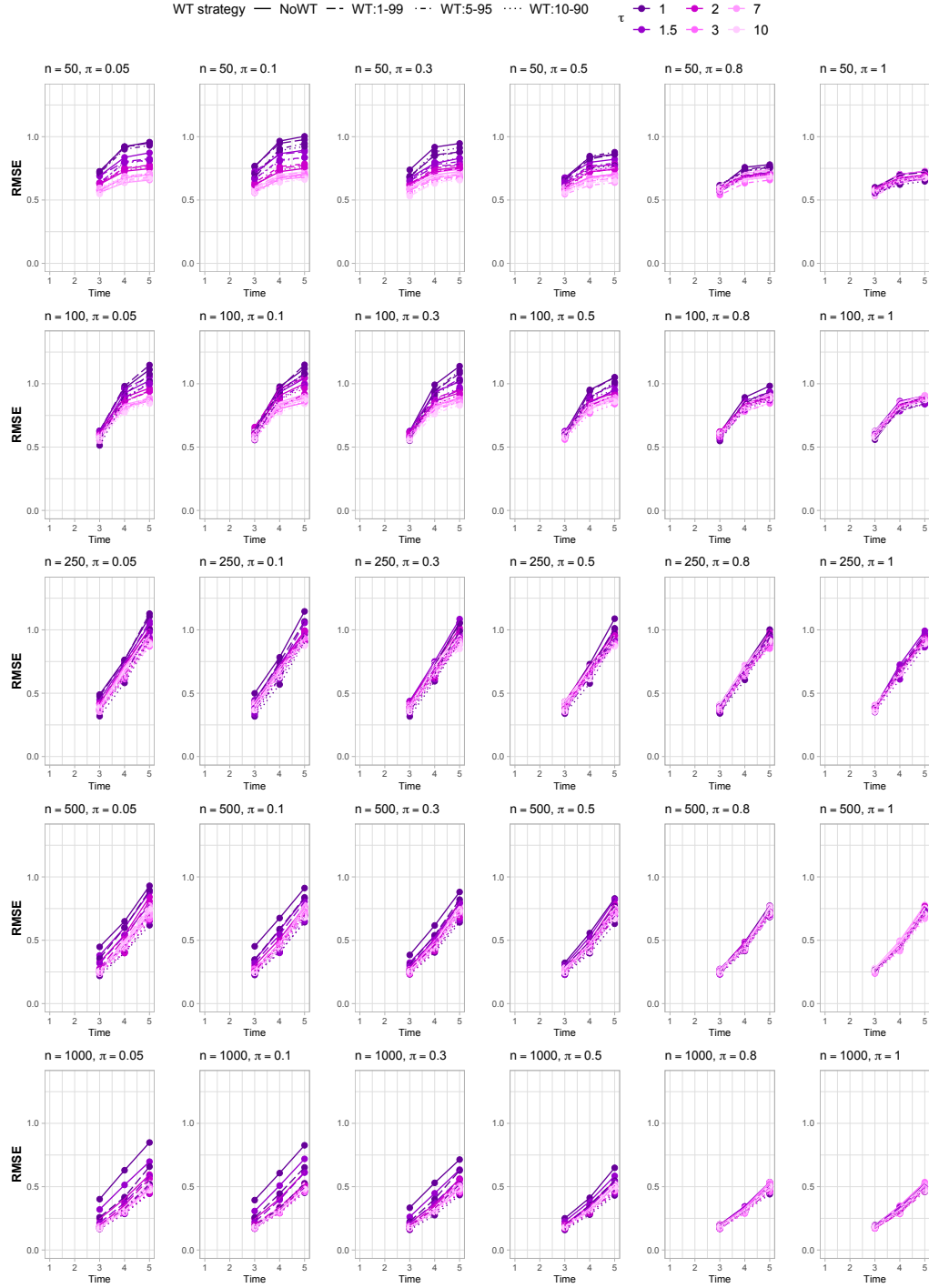


**Figure S19:** Root Mean Squared Error (RMSE) of the estimates for the cumulative coefficient  $C_{A_2}(t) = \int_2^t \tilde{\alpha}_{A_2}(s)ds$  at time points  $t = 3, 4, 5$  for the different setting of simulation study II. Each row refers to a different sample size  $n = 50, 100, 250, 500, 1000$ . Each column refers to a different exposure cut-off  $\pi = 0.05, 0.1, 0.3, 0.5, 0.8, 1$ . Different types of line refer to different weight truncation (WT) strategies (solid: No WT; long-dashed: 1-99 WT; dot-dashed: 5-95 WT; dotted: 10-90 WT). The colours refer to different values of the rule-threshold  $\tau$ : the darker the colour, the more severe the violation (i.e., the lower  $\tau$ ).



## RMSE for $\hat{C}_{A_3}(t)$ estimated from Aalen-MSM (12)

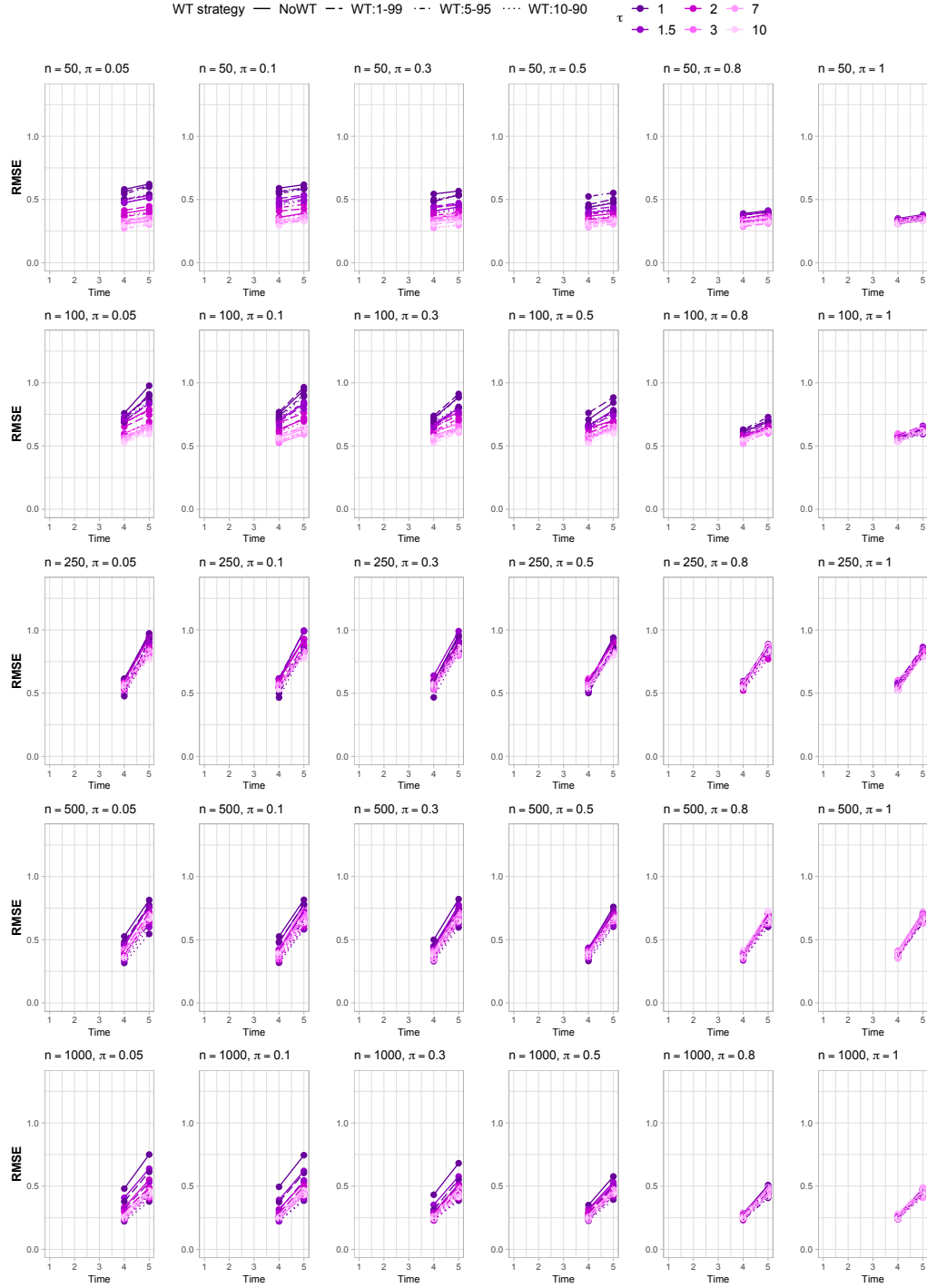


**Figure S20:** Root Mean Squared Error (RMSE) of the estimates for the cumulative coefficient  $C_{A_3}(t) = \int_3^t \tilde{\alpha}_{A_3}(s) ds$  at time points  $t = 4, 5$  for the different setting of simulation study II. Each row refers to a different sample size  $n = 50, 100, 250, 500, 1000$ . Each column refers to a different exposure cut-off  $\pi = 0.05, 0.1, 0.3, 0.5, 0.8, 1$ . Different types of line refer to different weight truncation (WT) strategies (solid: No WT; long-dashed: 1-99 WT; dot-dashed: 5-95 WT; dotted: 10-90 WT). The colours refer to different values of the rule-threshold  $\tau$ : the darker the colour, the more severe the violation (i.e., the lower  $\tau$ ).

# RMSE for $\hat{C}_{A_4}(t = 5)$ estimated from Aalen-MSM (12)

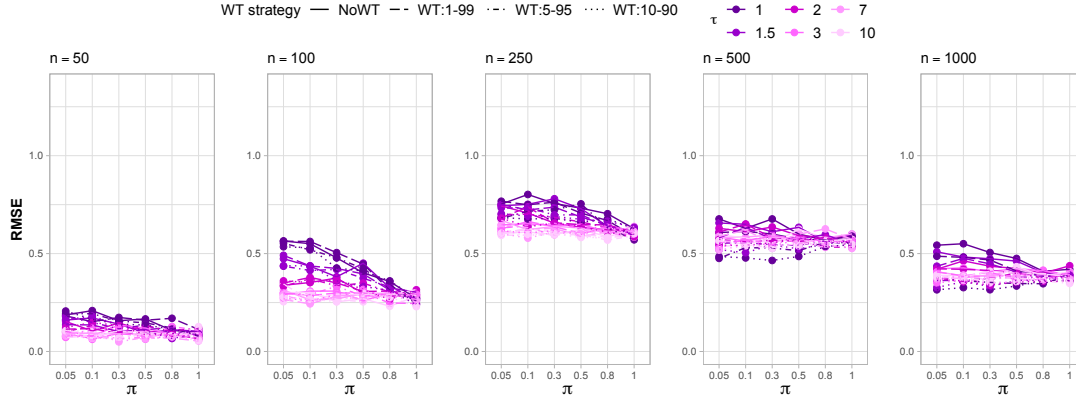


**Figure S21:** Root Mean Squared Error (RMSE) of the estimates for the cumulative coefficient  $C_{A4}(t = 5) = \int_4^5 \tilde{\alpha}_{A4}(s)ds$  for the different setting of simulation study II. Each column refers to a different sample size  $n = 50, 100, 250, 500, 1000$ . The x-axes show the compliance-threshold values  $\pi = 0.05, 0.1, 0.3, 0.5, 0.8, 1$ . Different types of line refer to different weight truncation (WT) strategies (solid: No WT; long-dashed: 1-99 WT; dot-dashed: 5-95 WT; dotted: 10-90 WT). The colours refer to different values of the rule-threshold  $\tau$ : the darker the colour, the more severe the violation (i.e., the lower  $\tau$ ).